THE ASTROPHYSICAL JOURNAL, 428:93–112, 1994 June 10

THE *HST* QUASAR ABSORPTION LINE KEY PROJECT. IV. *HST* FAINT OBJECT SPECTROGRAPH AND GROUND-BASED OBSERVATIONS OF THE UNUSUAL LOW-REDSHIFT BROAD ABSORPTION-LINE QUASI-STELLAR OBJECT PG 0043+039[1]

DAVID A. TURNSHEK,[2] BRIAN R. ESPEY,[2] MICHAEL KOPKO, JR.,[2] MICHAEL RAUCH,[3]
RAY J. WEYMANN,[3] BUELL T. JANNUZI,[4] ALEC BOKSENBERG,[5] JACQUELINE BERGERON,[6]
GEORGE F. HARTIG,[7] W. L. W. SARGENT,[8] BLAIR D. SAVAGE,[9]
DONALD P. SCHNEIDER,[4] AND ARTHUR M. WOLFE[10]
Received 1993 August 4; accepted 1993 November 11

ABSTRACT

HST FOS observations have shown that the spectrum of the low-redshift ($z_{em} \simeq 0.384$) QSO PG 0043+039 exhibits weak broad absorption lines (BALs). The BALs were discovered during the course of UV spectrophotometry made for the *HST* Quasar Absorption Line Key Project. The *HST* data are analyzed along with ground-based optical and *IUE* spectrophotometry. The object is found to have a number of atypical properties relative to normal non-BAL QSOs. For example, the object is one of the strongest Fe II emitters known, narrow-line [O III] and [O II] emission is not detected, and the C IV broad emission line is exceedingly weak. The observed continuum is atypical in the sense that it is much weaker than that of a normal optically selected QSO at rest wavelengths $\lesssim 2200$ Å. Intrinsic reddening of $E(B-V) \simeq 0.11$ mag by dust similar to that found in the SMC at the redshift of PG 0043+039 conservatively accounts for the observed continuum shape moderately well. These observed characteristics are typical of low-ionization BAL QSOs, but convincing evidence for BALs due to low-ionization transitions of Mg II, Al III, Al II, or C II does not exist. Therefore, this object may be a misaligned BAL QSO having many of the characteristics of low-ionization BAL QSOs with the sight line passing through a putative dusty region, but evidently missing clouds of high enough column density to produce observable low-ionization BALs. If the intrinsic dust-extinction model is correct, the observations suggest that the dust is not confined to the presumably higher density, low-ionization BAL clouds, but that it has drifted to nearby high-ionization BAL regions. We also consider other possible mechanisms for producing the shape of the continuous energy distribution which cannot be ruled out. We compare the Fe II emission in PG 0043+039 with that in another Key Project QSO, NGC 2841–UB 3, which has optical Fe II emission comparable in strength to that in PG 0043+039, but has anomalously weak UV Fe II emission. In addition, from an analysis of UV and optical spectrophotometric data at 5 epochs over ~ 11 yr, there is tentative evidence that PG 0043+039 has varied in brightness by as much as 1.1 mag during this time interval.

Two different interpretations of PG 0043+039 and the low-ionization BAL QSOs are considered: One is that the low-ionization BAL QSOs comprise a distinct population of QSOs that have large BAL region covering factor, no appreciable narrow emission-line region, and other atypical properties. An alternative possibility is that PG 0043+039 has a small BAL region covering factor, which is consistent with previously proposed models for most BAL QSOs, but that nonspherical geometries coupled with mechanisms for anisotropic emission give rise to aspect-angle dependent QSO spectral properties, such as weak narrow-line [O III] emission. While the actual value of the BAL region covering factor in PG 0043+039 and low-ionization BAL QSOs is unclear, given the absence of a specific model which would give rise to anisotropic continuum or line emission of the type required, the evidence presented here would seem to indicate that the BAL region covering factor in a subclass of QSOs is larger than resonance line scattering models generally indicate. Various model scenarios for explaining the weak narrow-line [O III] emission are considered, but there is no definitive explanation.

Subject headings: galaxies: Seyfert — quasars: absorption lines — quasars: individual (PG 0043+039) — ultraviolet: galaxies

[1] Based on observations with the NASA/ESA *Hubble Space Telescope*, obtained at the Space Telescope Science Institute, which is operated by the AURA, Inc., under NASA contract NAS 5-26555, with the NASA *IUE* Satellite, with the NOAO KPNO 4 m Telescope, which is operated by AURA, Inc., under agreement with NSF, and with the Palomar 5 m Hale Telescope, under a cooperative agreement between the Carnegie Institution of Washington and the California Institute of Technology.

[2] Department of Physics and Astronomy, University of Pittsburgh, Pittsburgh, PA 15260.
[3] OCIW, 813 Santa Barbara Street, Pasadena, CA 91101.
[4] Institute for Advanced Study, School of Natural Sciences, Princeton, NJ 08540.
[5] Royal Greenwich Observatory, Madingley Road, Cambridge CB3 0EZ, England.
[6] Institut d'Astrophysique de Paris, CNRS, 98 bis, boulevard Arago, F-75014 Paris, France.
[7] Space Telescope Science Institute, 3700 San Martin Drive, Baltimore, MD 21218.
[8] Mail Code 105-24, California Institute of Technology, Pasadena, CA 91125.
[9] Department of Astronomy, University of Wisconsin, Madison, WI 53706.
[10] CASS, University of California at San Diego, La Jolla, CA 92093.

1. INTRODUCTION

Broad absorption-line (BAL) QSOs are a subclass of QSOs that show mostly highly ionized gas flowing away from the central source at speeds up to 30,000 km s^{-1} or more. Studies of them may provide information on QSO geometries, the production of metals in the young universe, the physics of the outflows, and ultimately how the outflows affect a QSO's surrounding environment. During the course of the *HST* Quasar Absorption-Line Key Project observations, we discovered that the low-redshift ($z_{em} \simeq 0.384$) QSO PG 0043+039 has weak BALs (Bahcall et al. 1993). In this paper we summarize these observations, report on additional observations which span from UV to radio wavelengths, along with spectra of another Key Project QSO, NGC 2841–UB 3, and discuss the implications.

BALs appear in the spectra of $\sim 10\%$ of all radio-quiet QSOs at all redshifts. The most recent review of observational work, conclusions, and concepts for models is by Turnshek (1988), while Weymann, Turnshek, & Christiansen (1985) discuss mechanisms for accelerating the outflows. More recent results are reported by Junkkarinen, Burbidge, & Smith (1987), Turnshek et al. (1987, 1988), Hazard et al. (1987), Morris (1988), Barlow, Junkkarinen, & Burbidge (1989), Kwan (1990), Weymann et al. (1991), Begelman, De Kool, & Sikora (1991), Sprayberry & Foltz (1992), Stocke et al. (1992), Boroson & Meyers (1992), Barlow et al. (1992), Korista et al. (1992), Hamann, Korista, & Morris (1993), and Voit, Weymann, & Korista (1993). Appendix A of Weymann et al. (1991) suggests an objective, albeit ad hoc, procedure for deciding which QSOs to classify as BAL QSOs. While most BAL QSOs show only high-ionization BALs in their spectra, $\sim 5\%$–15% of them also exhibit low-ionization BALs.[11] We first summarize some of the results that have come from observations of high-ionization BAL QSOs.

BALs are observed because inner continuum photons, and, in some cases, inner broad emission-line (BEL) region photons are scattered by the resonance lines from BAL region clouds. Based on the *estimated* optical depths and electron densities, only a very small fraction of the scattered photons should be destroyed by absorption and reprocessing. However, profile analysis suggests that significant numbers of resonance line scattered photons are not present (see Hamann et al. 1993 for a recent analysis). These results indicate that either other mechanisms act to destroy the photons, or else typical BAL region covering factors are $\lesssim 0.2$. In the latter case, since the fraction of QSOs with BALs is $\sim 10\%$, the upper limit on the covering factor implies that many, perhaps most, QSOs have BAL regions.[12] At the same time, statistical studies reveal differences between BAL and non-BAL QSOs with respect to their optical polarization and some of their BEL properties. Strong radio sources and BAL QSOs also seem to be mutually exclusive. Plausible explanations for these differences include non-spherical BAL region geometries, correlated anisotropic emission from the continuum or line-emitting regions of QSOs, characteristically different populations of QSOs, or a combination of these effects. The inference that most luminous QSOs intrinsically have BAL regions, which is inferred from the small covering factor constraint, argues against the notion of two separate populations of QSOs—BAL QSOs and non-BAL QSOs—at least among the radio-quiet population of QSOs. If a small covering factor is accepted, additional evidence for an asymmetric, nonspherical large-scale distribution of BAL gas comes from the high incidence of multiple absorption troughs seen in the spectra, which may arise from discrete episodic events. Thus, at least for the high-ionization BAL QSOs, available results indicate that disklike or jetlike large-scale BAL region geometries, possibly coupled with mechanisms for anisotropic emission correlated with the geometry of the BAL region, is a promising way to interpret the observed systematics of BAL QSO properties (e.g., see the suggestions of Turnshek 1988 or Hamann et al. 1993 for two possibilities).

The situation for low-ionization BAL QSOs is different, however, and the finding that the BAL region covering factor is small may not apply to them. The study of Boroson & Meyers (1992) indicates that low-redshift, low-ionization BAL QSOs may systematically have weak narrow-line [O III] emission and that nearly all of the QSOs in their *IRAS*-selected sample which lack narrow-line [O III] emission may have low-ionization BALs. If narrow-line [O III] is emitted isotropically (but see Netzer & Laor 1993 and Hes, Barthel, & Fosbury 1993), one expects the low-ionization BAL region covering factor to simply be the fraction of weak narrow-line [O III] QSOs which have low-ionization BALs. Boroson & Meyers (1992) suggest that this fraction approaches unity in their *IRAS*-selected sample and that at least the low-ionization BAL QSOs must constitute a separate population of QSOs with large BAL region covering factor. However, as discussed in § 4, conclusions resulting from more generally considering the [O III] emission in non–*IRAS*-selected samples are mixed on this point and may indicate covering factors considerably smaller than unity.

One way to reconcile the results of Boroson & Meyers (1992) with a small covering factor, single-population model is to postulate some correlation between the large-scale geometry of the BAL region and the regions which normally give rise to the observed narrow-line [O III] emission or the continuum and broad-line emission. For example, in such a unified model, there would have to be some mechanism which prevents [O III] emission from escaping the QSO in the direction of BAL region clouds or which causes enhanced continuum and broad-line emission in the direction of BAL region clouds. But while the actual value of the BAL region covering factor in PG 0043+039 and low-ionization BAL QSOs is unclear, the evidence presented here suggests that it is larger than the scattering models suggest (see § 4). Sprayberry & Foltz (1992) also consider the problem of incorporating the low-ionization BAL QSOs into a single-population, unified model.

In addition to issues involving the BAL region covering factor are ones which deal with size scales and physical conditions. The observations show that the BAL gas occults the Lyα BEL gas, hence the BAL region must lie beyond this region. Significant *broad* [O III] $\lambda\lambda$4959, 5007 emission does not originate in the BAL region, which suggests an electron density $n_e \gtrsim 10^6$ cm^{-3}. Photoionization equilibrium calculations then indicate that the BAL region *must lie within* 30–500 pc of the

[11] We emphasize that the term "low-ionization BAL QSO" does not imply that only low-ionization material is present. We are unaware of objects which could be called BAL QSOs which show *only* low-ionization BALs. Most low-ionization BAL QSOs have a tendency to have stronger high-ionization BALs than those seen in QSOs only exhibiting high ionization BALs. When generically referring to a low-ionization BAL QSO, we mean that BALs due to one or more of the following transitions appear in the spectrum: Mg II, Al III, Al II, and/or C II.

[12] While only a small fraction of QSOs are *observed* to have BALs in their spectra, results on the covering factor indicate that many of the QSOs that are not observed to have BALs in their spectra must be intrinsic BAL QSOs.

central source for the usual range of QSO luminosities. Moreover, the BAL profile properties appear to be correlated with those of the BEL profiles, suggesting that the BAL region is somehow related to the BEL region. A straightforward analysis of BAL profiles suggests that metal abundances in BAL regions may be greatly enhanced relative to solar abundances, but issues concerning incomplete source coverage by individual BAL clouds and their thermal and ionization structure need to be studied more thoroughly before the degree of enhancement is fully understood.

The foregoing constraints form the basis for an empirical, albeit static, model. Questions dealing with the origin, evolution, and consequences of BAL outflows are not presently part of any well-developed model. However, given the small sizes that are inferred for the distance between the central source and the outflowing BAL gas, which implies short times for clouds to cross the region compared to QSO lifetimes, the most reasonable scenario might be a steady wind which is perturbed by episodic events. Within the framework of the constraints just outlined, supernovae, perhaps confined to a disk or jetlike region, may explain both enhanced abundances and episodic events.

The purpose of this paper is to consider the implications of the PG 0043+039 observations. The properties that PG 0043+039 exhibits—negligible narrow-line [O III] emission, very strong Fe II emission, and a strong deficit of flux in the UV—are shared by the low-ionization BAL QSOs. However, PG 0043+039 has much weaker C IV BALs, and it does not show any clear evidence for the low-ionization BALs. We suggest, therefore, that an understanding of PG 0043+039 might provide clues to the nature of BAL QSOs in general and low-ionization BAL QSOs in particular, and consider various scenarios to interpret the PG 0043+039 observations. The observations are presented in § 2, the analyses of these observations are presented in § 3, and their implications are discussed in § 4. We give a brief summary of our conclusions and suggestions for further work in § 5.

2. OBSERVATIONS

2.1. *Ultraviolet Spectrophotometry*

HST-FOS spectra of PG 0043+039 covering from ~1600 to 3270 Å were obtained with the FOS G190H and G270H gratings on 1991 October 28, as part of the Quasar Absorption-Line Key Project Survey (Table 1). Bahcall et al. (1993) present a study of the narrow absorption lines present in the spectra (see their Fig. 1 and Table 6). The data processing and the algorithm for identifying the narrow absorption-line systems are described in Schneider et al. (1993). Since Bahcall et al. optimized their analysis techniques for detection and study of narrow absorption-line systems, their continuum fit of the PG 0043+039 spectrum follows both the BELs and BALs; thus the observable weak BALs are not found by their line selection and identification software, and they are not readily apparent in the published spectrum.

In Figure 1 we present a composite of the spectrum of PG 0043+039 consisting of the joined FOS G190H and G270H observations, together with the ground-based optical spectra discussed in § 2.2. The spectrum has been shifted into the rest frame assuming a redshift of 0.384 based on the optical data presented in § 2.2. The observed UV lines were deemed less reliable for deriving the redshift because the data were inferior in terms of signal-to-noise ratio characteristics, strength of features, and contamination from Fe II emission. The UV spectrum of PG 0043+039 is unlike most other QSO/AGN spectra because it exhibits an atypical continuum which is much weaker than that of a normal optically selected QSO at rest wavelengths $\lesssim$2200 Å (see § 3.1) and evidence for an extremely strong broad complex of emission longward of ~2000 Å which is almost certainly due to Fe II (see § 3.2.1). A very weak C IV λ1549 BEL and unusually strong BEL near λ1309 and λ1260 are also present (see § 3.2.2). In addition, weak BALs due to C IV $\lambda\lambda$1548, 1550 and Si IV $\lambda\lambda$1393, 1402 are present (see § 3.3), but there is no significant evidence for weak BALs due to Al III $\lambda\lambda$1857, 1863. BALs due to C II λ1335 or Al II λ1670 are also not observed, but they would be unlikely given the absence of Al III. The lack of coverage shortward of the Lyα/N V broad emission lines prevents an adequate search for Lyα and N V BALs. Measurement of the Figure 1 spectrum suggests that the C IV BAL is present over a velocity interval of ~5000–17,000 km s^{-1}. The C IV, Si IV, and Al III BAL labels on Figure 1 correspond to this velocity interval.

Two UV observations of PG 0043+039 were also made with the *IUE* satellite between 1986 November and 1987 January. The optimally processed and co-added *IUE* data appear in the recent compilation of archival *IUE* QSO/AGN spectra by Lanzetta, Turnshek, & Sandoval (1993). Based on the *IUE* spectrum, PG 0043+039 could not be identified as a BAL QSO. These *IUE* observations are discussed in § 3.4 in connection with the possibility of brightness variations in PG 0043+039.

2.2. *Ground-based Optical Spectrophotometry*

We have obtained several ground-based optical spectra of PG 0043+039, the details of which are presented in Table 1. Low-resolution, high signal-to-noise ratio Palomar 5 m data were obtained over the entire optical wavelength range with the Double Spectrograph (Oke & Gunn 1982), while higher resolution, lower signal-to-noise ratio KPNO 4 m data were obtained near Mg II with the RC Spectrograph and 1024 by

TABLE 1

JOURNAL OF SPECTROSCOPIC OBSERVATIONS

Telescope	Instrument	Date	Exposure Time (s)	Coverage (Å)	Resolution (Å)
KPNO 4 m	RC Spectrograph	1991 Oct 27	2700	3250–4000	1.6
HST 2.5 m	FOS/RD/G190H	1991 Oct 28	2960	1600–2250	1.5
HST 2.5 m	FOS/RD/G270H	1991 Oct 28	1050	2300–3270	2.1
Palomar 5 m	DS/Blue[a]	1991 Dec/1992 Oct	1430	3250–4680	5.3
Palomar 5 m	DS/Red[a]	1991 Dec/1992 Oct	4420	4680–9100	13.8

[a] Double Spectrograph Blue Side or Double Spectrograph Red Side.

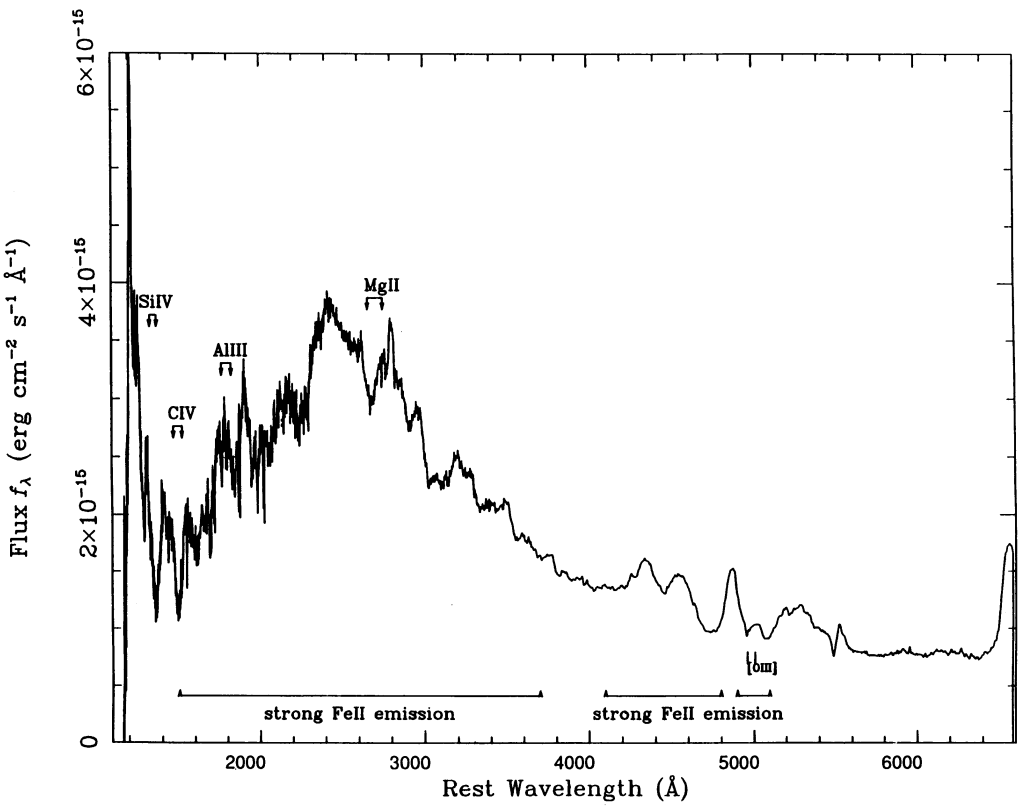

FIG. 1.—The spectrum of PG 0043+039 obtained with the *HST* FOS G190H and G270H gratings from 1600 to 3250 Å and with the Palomar 5 m Double Spectrograph from 3250–9100 Å in the observed frame. The spectral resolution is ~250 km s^{-1} for the *HST* portion of the spectrum, ~400 km^{-1} for the blue channel portion of the Double Spectrograph spectrum (3250–4680 Å) and ~600 km^{-1} for the red channel (4680–9100 Å). The plotted spectrum has been shifted to the rest frame using a redshift of 0.384. The label corresponding to the C IV $\lambda\lambda$1548, 1550 BAL runs from an outflow velocity of 5000 km s^{-1} up to 17,000 km s^{-1}. This is used to predict the position of possible BALs due to Si IV $\lambda\lambda$1393, 1402, Al III $\lambda\lambda$1857, 1863, and Mg II $\lambda\lambda$2796, 2802. The presence of the C IV and Si IV BALs is apparent, but the Al III and Mg II regions are used to place upper limits on possible absorption.

1024 Tektronix CCD detector. Our optical spectra allow us to derive an emission redshift of $z_{em} = 0.384 \pm 0.002$ from the observed Mg II ($z_{em} = 0.383$), Hβ ($z_{em} = 0.386$), and Hγ ($z_{em} = 0.382$) emission lines which are consistent with determinations from earlier ground-based optical spectra (Baldwin, Wampler, & Gaskell 1989; Boroson & Green 1992). The earlier ground-based spectra are considered in § 3.4 in connection with possible brightness variations. Both the Palomar and KPNO data were processed and flux calibrated using the IRAF software packages.[13] The absolute flux calibrations were accomplished with the aid of short-exposure wide-slit observations on those nights when it appeared to be photometric. The Palomar optical data are shown along with the *HST* UV data in Figure 1 with the predicted position of Mg II BALs over the velocity interval 5000–17,000 km s^{-1} labeled. The KPNO 4 m spectrum of the Mg II region is shown in Figure 2 with the predicted position of Mg II BALs labeled. In many QSO spectra, the presence of Fe II emission gives rise to an apparent depression just shortward of the Mg II BEL which could be mistaken for broad absorption. In fact, the analysis in § 3 will show that *the optical spectra of PG 0043+039 reveal no clear indication of* Mg II *BALs.* An upper limit on the Mg$^+$ BAL region column density is derived in § 3.3.

[13] IRAF is distributed by NOAO, which is operated by AURA, Inc., under contract to the NSF.

2.3. *Previously Published Results on the Spectral Energy Distribution of PG 0043+039 from UV to Radio Wavelengths*

Since PG 0043+039 may be related to a class of objects having infrared and other properties of particular interest, as discussed in § 4, we also consider other available information from UV, optical, infrared, and radio wavebands. PG 0043+039 was not observed with *Einstein* in the X-ray region, but Schmidt & Green (1986) discuss its expected X-ray flux. Figure 3 illustrates earlier epoch observations of the overall spectral energy distribution of PG 0043+039: 1986/7 *IUE* UV observations (Sun & Malkan 1989; Lanzetta et al. 1993), 1980 optical and infrared observations (Neugebauer et al. 1989; Sun & Malkan 1989), 1983 *IRAS* infrared observations (Sanders et al. 1989), and 1982/3 6 cm VLA radio observations (Kellermann et al. 1989). PG 0043+039 was not detected with *IRAS*, and so upper limits on its flux in those wavebands are plotted.

Inspection of the large-scale spectral energy distribution of PG 0043+039 shown in Figure 3 does not reveal any grossly atypical properties such as a large infrared excess.

3. ANALYSIS

Analyses of the observations of PG 0043+039 discussed in § 2 yield information on the detailed spectral energy distribution and strength of emission lines, BAL region column den-

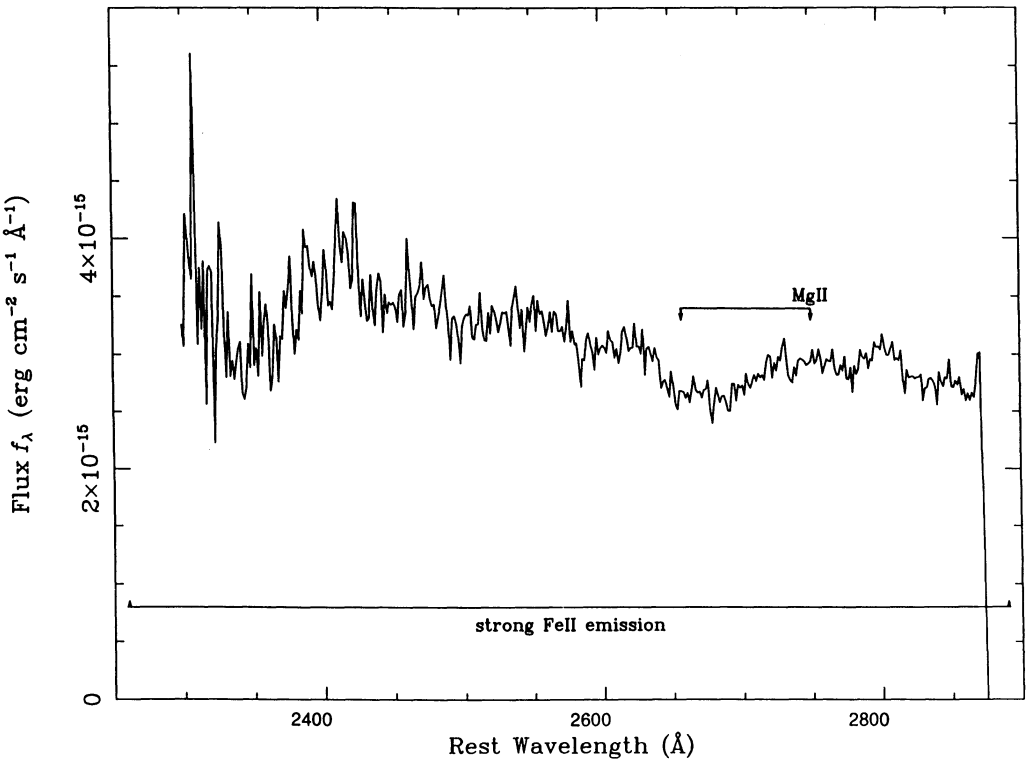

FIG. 2.—Rest frame spectrum of PG 0043+039 obtained with the KPNO RC spectrograph from 3250 to 4000 Å at a spectral resolution of ~130 km s^{-1}. The predicted position of a possible Mg II BAL (see Fig. 1) is labeled.

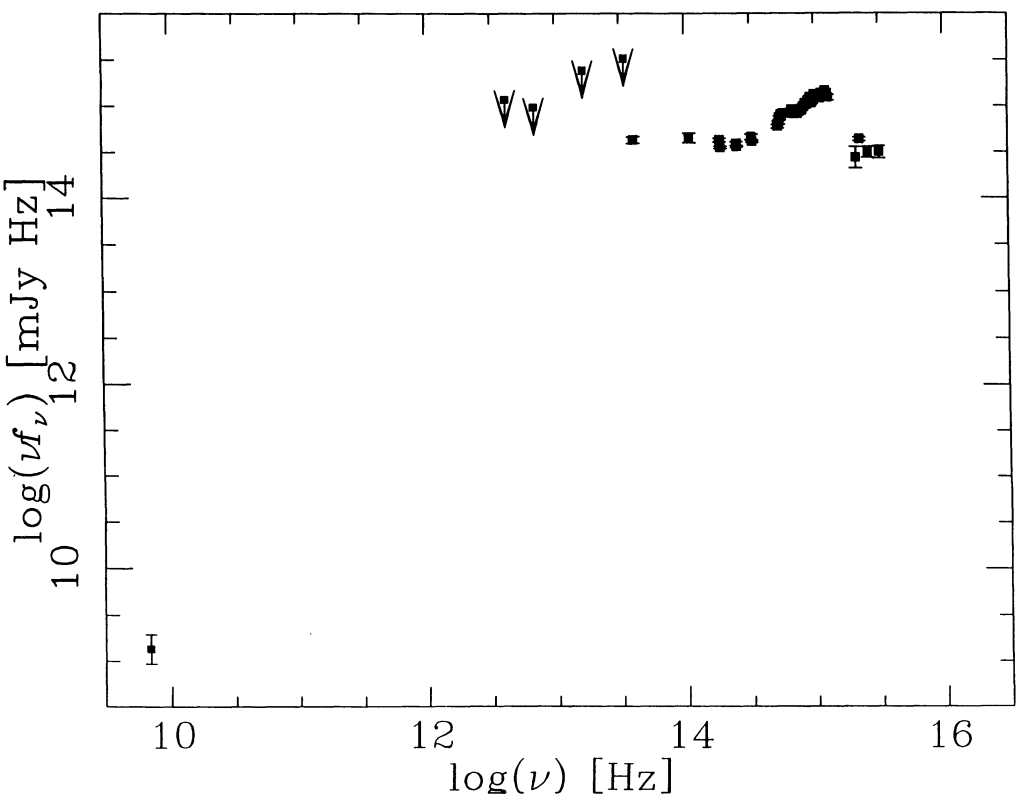

FIG. 3.—The multiwavelength spectral energy distribution of PG 0043+039 from UV to radio wavelengths using results from *HST*, optical telescopes, *IRAS*, and the VLA as described in § 2.3 and indicated on the figure.

sities, and possible brightness variations. In this section we summarize the results of these analyses.

3.1. *Continuous Energy Distribution in the UV and Optical*

Since the analysis that will be presented in § 3.1.1 suggests that intrinsic dust reddening may be significant in PG 0043+039, an important first step is to extinction-correct the PG 0043+039 spectral energy distribution using the most probable values for the Galactic extinction. The Galactic extinction correction will extend down to ~1600 Å in the observed frame. The best available Galactic H I column density estimate along our line of sight is $N(\mathrm{H\ I}) \simeq 3.0 \times 10^{20}$ cm^{-2} (Lockman & Savage 1993, as quoted in Savage et al. 1993). We have used this value together with the relation $E(B-V) = (5.53 \times 10^{21}\ \mathrm{cm}^{-2})^{-1}[N(\mathrm{H\ I})]$ mag, appropriate to lower column density sight lines (Diplas & Savage 1993), to obtain a reddening value of $E(B-V) = 0.055$ for PG 0043+039. This reddening value is higher than the upper limit of $E(B-V) < 0.03$ obtained for the same region from the Burstein & Heiles (1982) reddening maps. However, while the material seen along our line of sight to PG 0043+039 may actually be broken up into smaller clumps with a lower overall dust-to-gas ratio, for the purpose of examining the importance of reddening intrinsic to the QSO (see next section) the adoption of a larger Galactic correction factor results in more conservative estimates. We have thus adopted an $E(B-V)$ of 0.055 for the extinction correction of the UV/optical spectrum of PG 0043+039 and the remainder of our analysis we will be made with reference to this corrected spectrum.

3.1.1. *Evidence for Reddening by Dust*

In Figure 4 we show the same spectrum as in Figure 1 corrected for the probable Galactic extinction and superimpose on it a composite spectrum of optically selected QSOs taken from the Large Bright Quasar Survey (LBQS) (Morris et al. 1991 and references therein). This composite is itself the joining of two composite spectra, namely an extension of the "sample 1′" mean spectrum of Weymann et al. (1991) together with the mean of a set of 5 m Double Spectrograph spectra of LBQS objects having a narrow range in redshift and luminosity and covering from ~2000–5700 Å in the rest frame (Korista et al. 1994). These two composite spectra overlap from ~2000–3200 Å and in this overlap region the agreement is excellent. The flux scales of the composite spectrum and the PG 0043+039 spectrum have been adjusted so that the two fluxes agree at ~5600 Å. Figure 4 shows that PG 0043+039 has a continuous energy distribution which is strongly deficient in flux shortward of ~2200 Å. This behavior is similar to that found for the subset of BAL QSOs showing low-ionization BALs (Weymann et al. 1991) and has been interpreted in these objects as due to *intrinsic* reddening by SMC-like dust (Sprayberry & Foltz 1992). Following these authors, and after making the most probable correction for Galactic extinction (§ 3.1), we have made an attempt to deredden the spectrum of PG 0043+039 using an SMC extinction curve based on the functional form derived by Pei (1992). This is done by applying various amounts of intrinsic SMC-like reddening to the PG 0043+039 spectrum and trying to match its continuum with the composite spectrum. In principle,

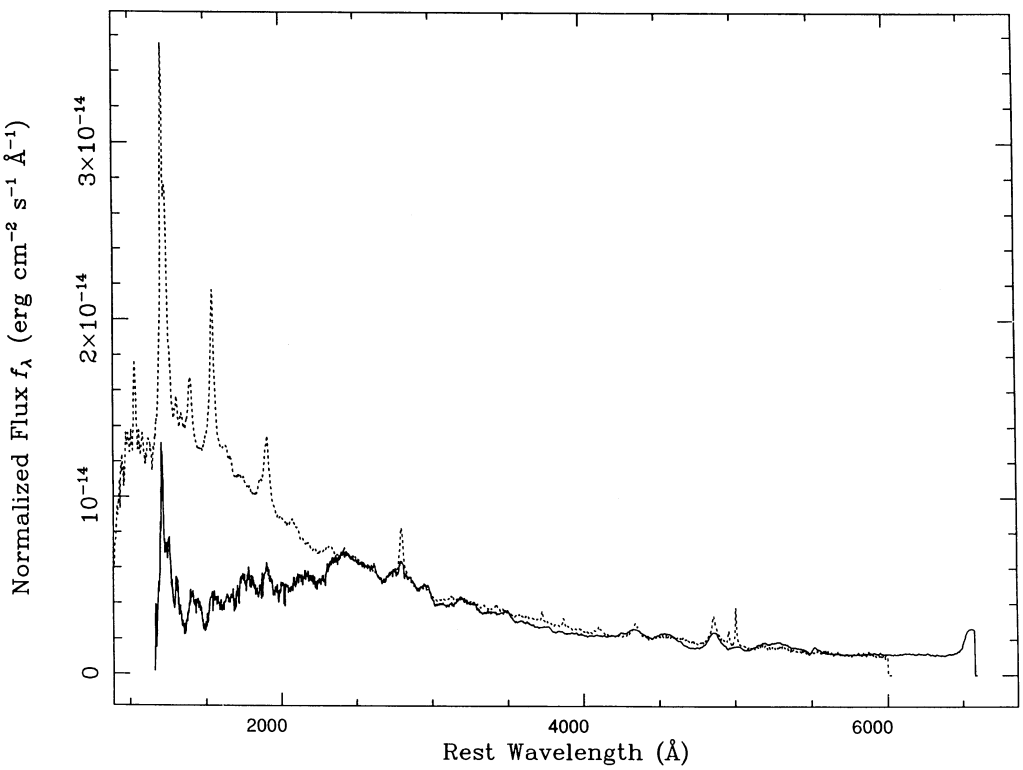

FIG. 4.—The rest frame spectrum of PG 0043+039 shown in Fig. 1 with the composite spectrum of optically selected QSOs derived from the LBQS survey superposed on it as described in § 3.1.1. The PG 0043+039 spectrum has been extinction-corrected for Galactic reddening by dust with $E(B-V) = 0.055$ mag. The flux scales are adjusted so they agree at ~5600 Å. The continuous energy distribution of PG 0043+039 is seen to have a relative deficit of flux at wavelengths shortward of ~2200 Å.

before doing this, we should also correct the composite spectrum by some appropriate mean Galactic reddening. In practice, however, this correction is less important for the composite spectrum because the data between *rest* wavelengths of $\sim$1200–2000 Å in the composite spectrum are based on optically selected QSOs whose typical redshift is $\sim$2.1; hence this region corresponds to *observed* wavelengths of $\sim$3720–6000 Å. For PG 0043+039, however, the same rest wavelength interval corresponds to $\sim$1600–2800 Å in the observed frame, so that correction for Galactic extinction in the region of interest will be greater for PG 0043+039 than for the composite spectrum. We therefore neglect any correction for Galactic extinction to the composite spectrum. We are also implicitly assuming that there is no evolution in the intrinsic spectral energy distribution of QSOs between redshifts of $\sim$2.1 and $\sim$0.3.

We find that *intrinsic* SMC-like reddening which produces $E(B-V) \simeq 0.11$ mag approximately accounts for the differences between the continuous energy distribution of PG 0043+039 and the non-BAL QSO composite spectrum. For example, if we consider "continuum points" in the rest wavelength intervals 1286–1297 Å, 1321–1336 Å, 1420–1463 Å, 4686–4744 Å, 5075–5100 Å, and 5700–5800 Å, then the continuum points in both the composite spectrum and the dereddened PG 0043+039 are consistent with a power law of approximately the same form. The SMC extinction-corrected spectrum of PG 0043+039 is shown in Figure 5 with the non-BAL QSO composite spectrum superposed on it. For SMC-like gas which has abundances that are $\sim$0.5 times solar values, the value $E(B-V) = 0.11$ implies a total H I column density of $N(\mathrm{H\ I}) \simeq 4.4 \times 10^{21}$ cm^{-2} (see Pei 1992).

3.1.2. *Alternative Explanations for the Continuous Energy Distribution*

Despite the success of the dereddening exercise discussed in § 3.1.1, alternative explanations for the shape of PG 0043+039's continuous energy distribution should be considered, because the presence of *intrinsic* reddening in PG 0043+039 is somewhat surprising given that the total observed BAL region column density appears to be significantly less than is normal for known BAL QSOs (§ 3.3). However, as we will suggest in § 4, along other directions the column density of both high- and low-ionization BAL material may be higher, and the dust may have drifted from these regions into our line of sight. In any case, based on the current observations we cannot demonstrate that intrinsic dust extinction is the only plausible explanation for the turndown in PG 0043+039's continuous energy distribution at rest wavelengths $\lesssim$2200 Å. In particular, we cannot rule out that PG 0043+039's observed spectrum and the observed spectra of low-ionization BAL QSOs are revealing something fundamental about how the synchrotron or thermal accretion disk spectrum is generated, possibly being a function of observer aspect angle, evolutionary state, some intrinsic QSO property, or some combination of these effects.

We have explored two possible alternative explanations for the continuous energy distribution of PG 0043+039: (1) a simple power law which is redder than the simple power-law that provides an acceptable fit to the non-BAL composite spectrum and (2) a power law plus accretion disk spectrum with the parameters adjusted to produce a reasonable fit to the PG 0043+039 spectrum. Both of these alternatives are meant to be illustrative rather than exhaustive. In conjunction with the work presented in § 3.2.1 on simultaneously fitting the under-

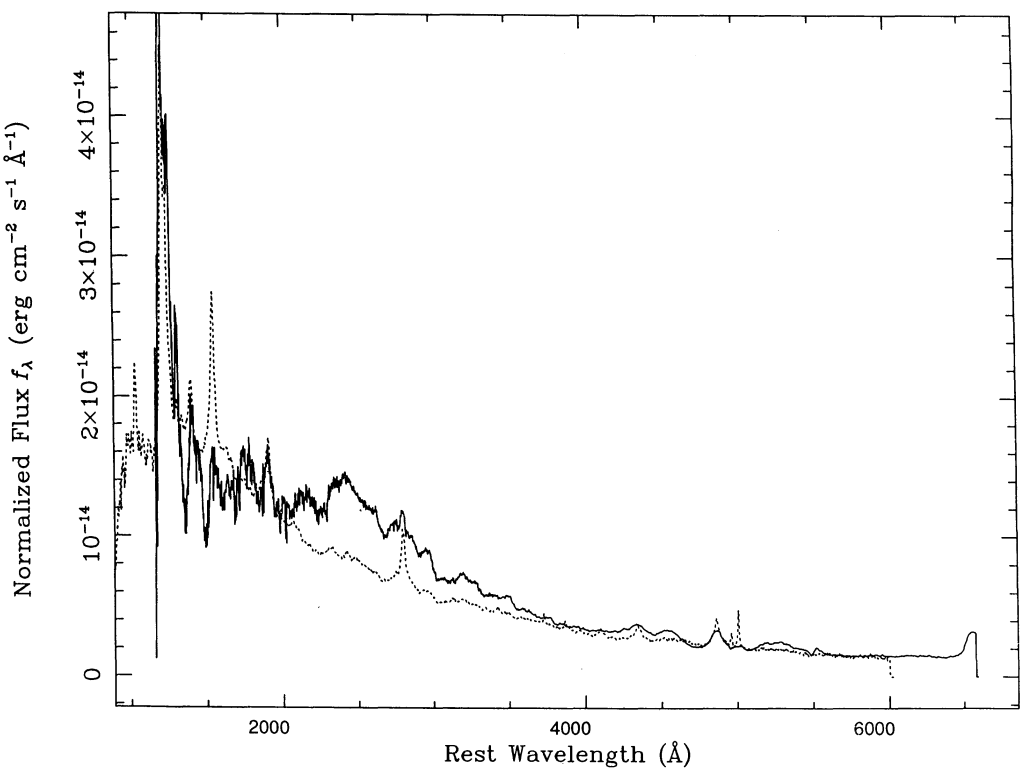

FIG. 5.—Same as Fig. 4 but with the PG 0043+039 spectrum additionally extinction-corrected for intrinsic reddening by SMC-like dust with $E(B-V) = 0.11$ mag.

lying continuum, Fe II emission, and Balmer and Paschen continua, we show that reasonable fits can be obtained for both cases. It should be kept in mind, however, that the template fitting methods which were used are not the result of a self-consistent model. In any case, the success of the final fits for the two alternatives which we consider suggest the need for additional observational and theoretical work before accepting the dust-extinction model.

For the case of a simple power law, the fitting program (see § 3.2.1) resulted in the selection of the simple power law shown in Figure 6*a*, with the remaining emission being attributed to Fe II emission, Balmer continuum emission, Paschen continuum emission, and other emission lines (see also Fig. 7*a* which is discussed in § 3.2.1). Consideration of this redder power-law continuum is relevant for the purposes of making a comparison to the composite LBQS spectrum and assessing viable alternatives to the intrinsic dust-extinction model.

For the case of the power-law plus accretion disk spectrum we considered the models of Laor & Netzer (1989) and ended up using a model very similar to the "best-fit" disk spectrum of Laor (1990). The basic model consists of two components: a "bare" thin accretion disk plus an underlying nonthermal power-law continuum. Laor provided us with the disk component part of his model fit which we adopted. However, to derive the slope and normalization of the power-law component we used the 10.1 μm observation of Sun & Malkan (1989) which was not included in the Laor fits. With regard to the disk component of the model alone, Laor (1990) has pointed out that his fit did not include the 2000–4000 Å rest wavelength region because of the obvious strong Fe II emission in that region; his fit to the data gives a χ^2 with the probability that it is acceptable. Laor (private communication) notes that the accretion disk by itself is very cold and gives rise to little ionizing flux. Figure 6*b* shows the power-law plus accretion disk continuum which we finally adopted as acceptable (see also Fig. 7*b* which is discussed in § 3.2.1). Notably, in this case the model employs a face-on accretion disk. A face-on accretion disk has the interesting property of giving rise to enhanced continuum in the direction perpendicular to the plane of the accretion disk since the apparent surface area of the disk is largest in this orientation. This type of enhancement would tend to reduce the observed equivalent width of the emission lines arising in a region which was emitting isotropically, such as might be the case for the narrow-line region. While it would be difficult to completely explain the very small [O III] emission equivalent widths using this scenario, such a model goes in the right direction and the PG 0043+039 observational results may further constrain such models.

3.2. *Emission-Line Strengths*

The very broad and strong Fe II emission, the presence of BAL features and the evidence for intrinsic dust extinction complicate establishing a continuum in PG 0043+039. However, the underlying continuum must be estimated in order to measure or constrain the emission and BAL features. The analyses of §§ 3.1.1 and 3.1.2 each suggest simple methods for establishing the underlying continuum, namely adopting a power-law continuum for the case where intrinsic dust extinction is important and adopting a power-law or a power-law plus accretion disk continuum for the case where intrinsic dust extinction is unimportant. For the case where intrinsic dust extinction is important, the moderately good agreement between the Lyα emission strength in the dereddened PG 0043+039 spectrum with the Lyα emission strength in the LBQS composite spectrum is consistent with the emission features being subject to approximately the same degree of extinction as the continuum. We will assume this to be the case, although this agreement could be fortuitous. Hence, we assume that the fluxes of the emission features depend inversely on the amount of intrinsic dust extinction. The equivalent widths of the emission features are independent of the amount of dust extinction, but depend on the details of the continuum fit. Tables 2 and 3, which present measurements of the spectrum in the framework of the various continuum models, serve to illustrate how the various measurements (e.g., equivalent widths) depend on the adopted continuum fit.

3.2.1. *Strength of the* Fe II *Emission*

Figures 5 and 6 make clear that PG 0043+039 has extremely strong Fe II emission in its optical and UV spectrum. Strong components of Balmer continuum emission and possibly Paschen continuum emission also appear to be present. Boroson & Green (1992) have made a measurement of the optical Fe II emission in PG 0043+039 and also conclude that it is unusually strong (see below). In an effort to provide a reasonably comprehensive assessment of the amount of Fe II emission in PG 0043+039, in Table 2 we present measurements of the strength of the Fe II emission relative to estimates of emission from other components using a variety of methods and for the various continuum models.

First, with the aid of theoretical model templates for the Fe II emission (see Wills, Netzer, & Wills 1985), Balmer continuum emission, and Paschen continuum emission which are described below, we present estimates of the Fe II emission flux, the Balmer continuum emission flux, the Paschen continuum flux, and the underlying continuum emission flux in three different rest frame wavelength intervals: 2000–3000 Å, 3000–3500 Å, and 3500–6000 Å. The Fe II emission flux is derived simply by subtracting the non–Fe II emission for the various continuum models. The total Fe II emission flux is determined from the sum of these measurements and is tabulated relative to the Hβ emission-line flux. The ratio of the Fe II emission flux relative to Hβ is of interest in the context of the energy budget problem (see § 4.3).

We used two Fe II emission-line templates in order to interpolate to one which approximated the data. The templates included one obtained from Netzer (1993) (the Netzer spectrum), and one similar to that generated by Wills, Netzer, & Wills to approximate the emission-line strengths seen in 3C 273. The Netzer spectrum was calculated for a larger optical depth at the Balmer limit and a larger turbulent velocity ($\tau_{BE} = 25$ and $v_{turb} = 10$ km s^{-1}) than was the case for the 3C 273 spectrum which has lower values of both parameters ($\tau_{BE} = 3.4$ and $v_{turb} = 2$ km s^{-1}). A larger optical depth at the Balmer edge results in more conversion of Fe II UV photons into Balmer photons (i.e., Fe II UV photons are destroyed by their photoionization of hydrogen in the $n = 2$ level) and a larger turbulent velocity inside the gas clouds reduces the pumping of optical Fe II transitions which lowers the optical to UV line strength (see Netzer & Wills 1983). The model spectrum of Netzer (1993) which was used here was broadened by convolution with Gaussians of varying widths to generate a library of Fe II templates. Optically thin Balmer and Paschen recombination continua as a function of temperature were also generated.

In order to fit the data, line-free regions were chosen in order to determine the power-law and recombination continua. Use

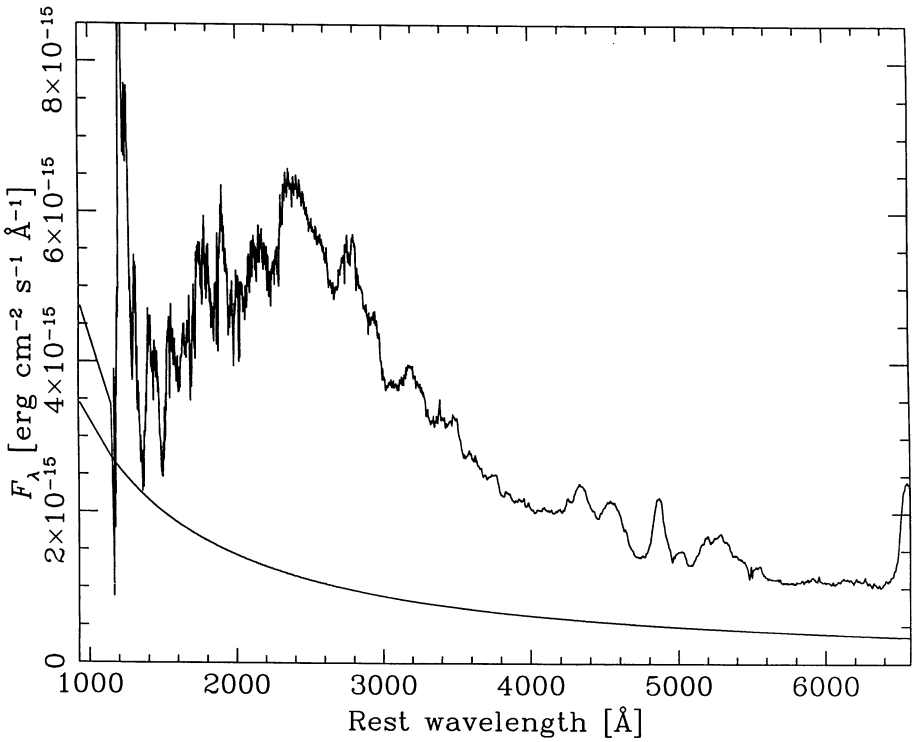

FIG. 6*a*

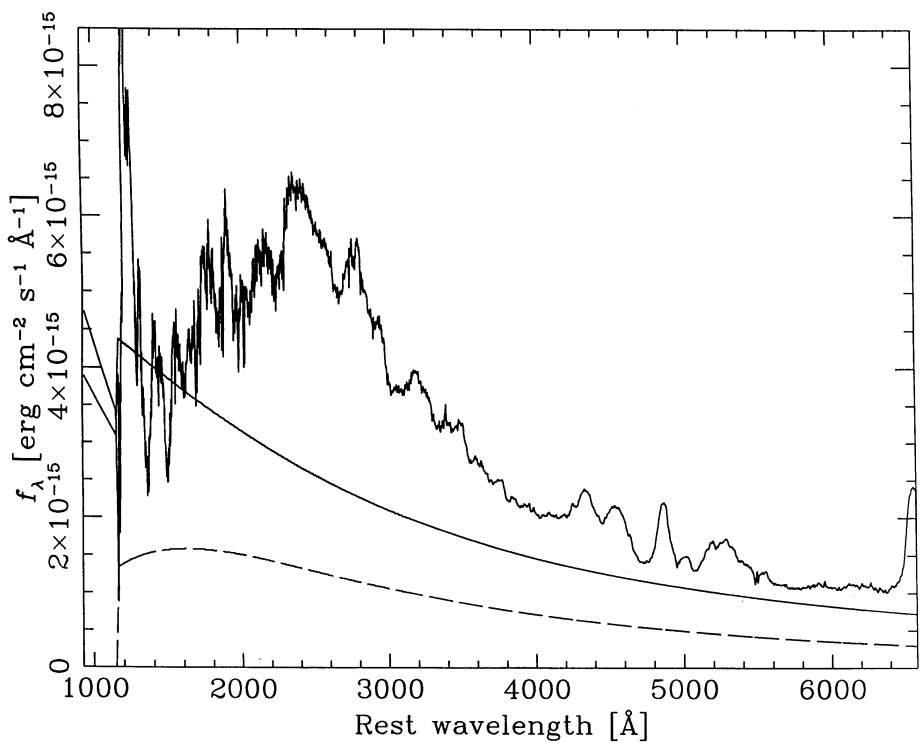

FIG. 6*b*

FIG. 6.—(*a*) The observed spectrum of PG 0043+039 without intrinsic dereddening and the simple power-law spectrum (*solid curve*) which was used in the fit to the continuous energy distribution shown in Fig. 7*a*. See the discussion in § 3.1.2. (*b*) The observed spectrum of PG 0043+039 without intrinsic dereddening and the power law plus accretion disk spectrum (*solid curve*) which was used in the fit to the continuous energy distribution shown in Fig. 7*b*. The accretion disk spectrum is also shown separately (*dashed curve*). See the discussion in § 3.1.2.

TABLE 2

Fe Emission, Balmer Lines, and Continuum Measurements

Type of Measurement	Model A[a]	Model B[b]	Model C[c]	Model D[d]
Fe II (2000–3000) flux[e]	441	183	214	70
Balmer continuum (2000–3000) flux[e]	39	109	54	50
Paschen continuum (2000–3000) flux[e]	~0	128	14	21
Underlying continuum (2000–3000) flux[e]	630	112	251	60
Fe II (3000–3500) flux[e]	63	29	34	11
Balmer continuum (3000–3500) flux[e]	46	50	40	21
Paschen continuum (3000–3500) flux[e]	~0	58	11	9
Underlying continuum (3000–3500) flux[e]	193	41	92	130
Fe II (3500–6000) flux[e]	61	42	38	35
Balmer continuum (3500–6000) flux[e]	26	19	21	50
Paschen continuum (3500–6000) flux[e]	6	216	64	20
Underlying continuum (3500–6000) flux[e]	519	133	289	596
Sum of fluxes of Balmer lines[f]	63	37	37	34
Fe II (total) flux[e]	565	254	286	116
Hβ flux[f]	9.1	6.0	6.0	5.0
Fe II (total)/Hβ flux ratio	62	42	48	23
Weymann et al. 1991 2400 Å REW Index[g] (Å)	59	59	59	22
Boroson & Green 1992 IZw1 template REW index[h] (Å)	109	109	109	37

[a] PG 0043+039 spectrum corrected for Galactic extinction with $E(B-V) = 0.055$ and intrinsic SMC-like dust extinction with $E(B-V) = 0.11$. The continuum has the form of a power law.

[b] PG 0043+039 spectrum corrected for Galactic extinction with $E(B-V) = 0.055$. The continuum has the form of a power law.

[c] PG 0043+039 spectrum corrected for Galactic extinction with $E(B-V) = 0.055$. The continuum has the form of a power law plus thermal accretion disk.

[d] LBQS composite spectrum. The continuum has the form of a power law. The LBQS composite spectrum has been scaled to bring it into rough agreement with the PG 0043+039 Hβ flux.

[e] The Fe II, Balmer continuum, Paschen continuum, and underlying continuum (power-law or power-law plus accretion disk) emission fluxes measured in three rest frame intervals from 2000–6000 Å after subtraction of the non–Fe II emission lines. The reported total Fe II emission flux is the sum of the three measurements. Fluxes are quoted in units of 10^{-14} ergs cm^{-2} s^{-1}.

[f] Also given in units of 10^{-14} ergs cm^{-2} s^{-1}.

[g] The emission rest equivalent width between rest wavelengths 2255 and 2650 Å as determined from the method of Weymann et al. 1991 which defines continuum windows at 2240–2255 Å and 2665–2695 Å.

[h] The Fe II emission rest equivalent width in the rest frame interval 4434–4684 Å, determined by broadening and fitting the I Zw 1 Fe II emission template spectrum, as reported by Boroson & Green 1992.

TABLE 3

Measurements of Other Emission Features

Transition	FWHM[a] (km s^{-1})	REW_{local}[b] (Å)	REW_a[c] (Å)	REW_b[d] (Å)	REW_c[e] (Å)	REW_d[f] (Å)
Lyα	5390	56	51	78	46	31
N V λ1240	4910	14	12	19	11	16
λ1260	7880	39	34	55	32	4
λ1309	7590	13	12	20	11	2
Si IV + [O VI] λ1400	7850	5	5	9	5	8
C IV λ1549	...	16	14	29	15	27
He II λ1640	4520	4	3	8	4	1
Mg II λ2800	3200	6	11	32	14	40
[O II] λ3727	...	0	0	0	0	2
Hγ/Fe blend	8580	27	37	99	45	27
Hβ	5400	56	62	166	77	58
[O III] λλ4959, 5007	...	0	0	0	0	19

[a] FWHM is the full width at half-maximum intensity in the PG 0043+039 spectrum relative to a locally established continuum.

[b] REW_{local} is the rest equivalent width measured in the PG 0043+039 spectrum relative to a locally established continuum.

[c] REW_a is the rest equivalent width measured in the PG 0043+039 spectrum corrected for Galactic extinction with $E(B-V) = 0.055$ and intrinsic SMC-like dust extinction with $E(B-V) = 0.11$ relative to a simple power-law continuum.

[d] REW_b is the rest equivalent width measured in the PG 0043+039 spectrum corrected for Galactic extinction with $E(B-V) = 0.055$ relative to a simple power-law continuum.

[e] REW_c is the rest equivalent width measured in the PG 0043+039 spectrum corrected for Galactic extinction with $E(B-V) = 0.055$ relative to the power-law plus thermal accretion disk continuum.

[f] REW_d is the rest equivalent width measure in the LBQS composite spectrum relative to a simple power-law continuum.

was made of the UV and infrared data of Sun & Malkan (1989) to determine the shape and intensity of the power-law component as these data agreed well with our spectra. With the continua held fixed, the Fe II emission strength was determined by interpolating between the two models mentioned above. While this will not result in a detailed fit to the data, approximation of the Fe II contribution was necessary in order to determine most of the other emission-line fits. The Fe II template spectra were then taken in turn by the χ^2 minimization fitting program (the Kriss SPECFIT package running in IRAF) and scaled to achieve the best fit to the data in the region of interest. A good fit over the wavelength interval 1460–6220 Å was achieved by broadening the theoretical Fe II template to $\gtrsim 8000$ km s^{-1}, which is broader than the characteristic FWHM of the Balmer and Mg II emission lines. The larger FWHM is probably related to the differences between the template Fe II spectrum and the data, rather than to a real difference between the FWHM of Fe II and Balmer emission lines. However, examination of the details of the fits shows that the local features are unlikely to be explained using a template FWHM as small as the locally measured Mg II value of 3200 km s^{-1}. Figures 7*a* and 7*b* show the fits to the data which can be obtained using the modified theoretical Fe II emission template superposed on Balmer and Paschen continuum components for the cases of an underlying continuum which is a simple power-law (Fig. 6*a*) and an underlying continuum which is a power law plus an accretion disk (Fig. 6*b*), respectively.

We wish to emphasize again, however, that while these fits are somewhat successful, they are meant to be illustrative. They should only be used as a starting point to further investigate models for the continuous energy distribution of PG 0043+039. In particular, the results that were presented in Table 2 are somewhat unique to the Netzer (1993) Fe II template that was utilized and the use of some other template might result in substantial differences in the estimated underlying continuum and the Balmer and Paschen continua. For example, the χ^2 minimizations sometimes result in Paschen continuum estimates that are almost certainly too high, and therefore most of this flux should probably be attributed to one of the other components.

As a further elaboration, we also point out that the original theoretical template of Wills et al. (1985) provides only a fair fit to the UV Fe II emission, and significant differences exist between the template and the observations. On the other hand, Figure 1 of Boroson & Green (1992) shows that the empirical I Zw 1 template provides a fairly good fit to the optical Fe II emission. The original Wills et al. theoretical Fe II emission template provides a rather poor fit to the optical Fe II emission.

Second, we present measurements of the index for UV Fe II emission at ~2400 Å as defined by Weymann et al. (1991), who used this index to measure the UV Fe emission in a sample of intermediate redshift normal and BAL QSOs. The algorithm which defines this index does not require a continuum to be fit, but uses predefined intervals to define a "pseudo-continuum." A similar index was also defined by these authors for a feature centered at ~2070 Å. This feature is usually strongly correlated in strength with the 2400 Å feature and may correspond to Fe III (see also Hartig & Baldwin 1986). However, the structure of the spectrum from ~2000–2200 Å is quite different in PG 0043+039 from other QSOs and a well-defined 2070 Å feature does not seem to exist. This may be due to the complex overlapping features.

Third, we present the index for optical Fe II emission as defined and reported by Boroson & Green (1992). Boroson & Green (1992) measured the optical Fe II emission by fitting an empirical Fe II template to their data. This template was generated by extracting the permitted optical Fe II lines from the narrow emission-line QSO I Zw 1, broadening them through convolution with a Gaussian of 5800 km s^{-1} (the width of the Hβ line in PG 0043+039), and then scaling it to the PG 0043+039 spectrum. This technique could not be applied to our UV observations as adequate data on QSOs/AGNs with strong narrow Fe II emission in the UV has not yet been published.

3.2.2. *Comparison of the* Fe II *Emission in PG 0043+039 and NGC 2841–UB 3*

The QSO NGC 2841–UB 3 (hereafter UB 3) was found by Arp (1981) during the course of a survey for QSOs near NGC 2841. The properties of this QSO have been discussed in detail by Sulentic, Zheng, & Arp (1990), who pointed out that it had unusually strong optical Fe II emission. They also suspected that UB 3 had unusually weak UV Fe II emission, given the strength of its optical Fe II. Coincidentally, UB 3 is a Key Project QSO for which FOS G190H and G270H spectra and Hale Telescope Double Spectrograph spectra have been obtained. Comparison of the spectra of PG 0043+039 and UB 3 is therefore of interest. Figure 8*a* shows the comparison in the rest frame between ~4000 and 5750 Å. UB 3 does indeed have optical Fe II emission which is comparable in strength to that observed in PG 0043+039. As pointed out by Sulentic et al. weak broad [O III] appears to be present; however, detailed modeling of the Fe II would be required to measure its strength. The emission from Hβ is quite strong, although its profile is badly distorted by the atmospheric A band, and the red side of the profile shown in Figure 8*a* is simply a guess as to its true shape.

Figure 8*b* shows the comparison of these same two objects over the rest frame interval ~1500–3500 Å and again shows the dramatic turndown in the far UV flux of PG 0043+039 which UB 3 clearly does not share. With the benefit of the FOS data, however, we can see that contrary to the speculation of Sulentic et al., UB 3 does show the characteristic signature of the UV Fe II emission from ~2250 to 2600 Å (see Fig. 8*b*). Measurement of the UV Fe II emission strength in UB 3 as measured by the 2400 Å index yields a value of 22 Å compared to 29 Å for the composite, so that while the UV Fe II emission is weaker than normal in UB 3, it is not dramatically so when compared to the mean of optically selected non-BAL QSOs. In fact, even in the optical, the composite spectrum has comparable Fe II emission around ~4570 Å, although the complex in the interval ~5100–5400 is ~3 times stronger in UB 3 than it is in the composite.

The 2400 Å index for PG 0043+039 is 59 Å (Table 2). If one compares this index with the values measured in the sample of 40 BAL QSOs (sample 2′) from Weymann et al. (1991), one finds that PG 0043+039 does indeed possess strong UV Fe II emission. Only two of the BAL QSOs from the sample have a larger 2400 Å index, while a third has a virtually identical index. However, the value of the index for PG 0043 is only ~1.3 σ above the mean for that sample.

As is clear from this and past work, the details of the Fe II emission processes in QSOs/AGN are complex.

3.2.3. *Other Emission-Line Properties*

Table 3 summarizes measurements of the main accessible non–Fe II emission lines of PG 0043+039 in terms of FWHM velocities and rest equivalent widths relative to a local contin-

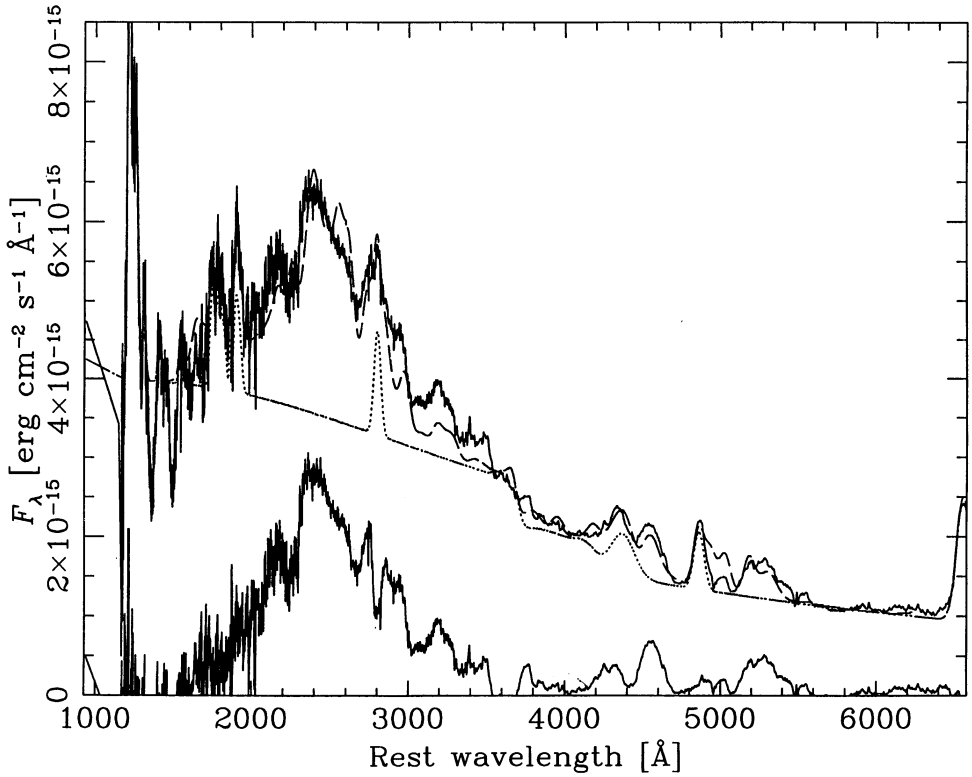

FIG. 7*a*

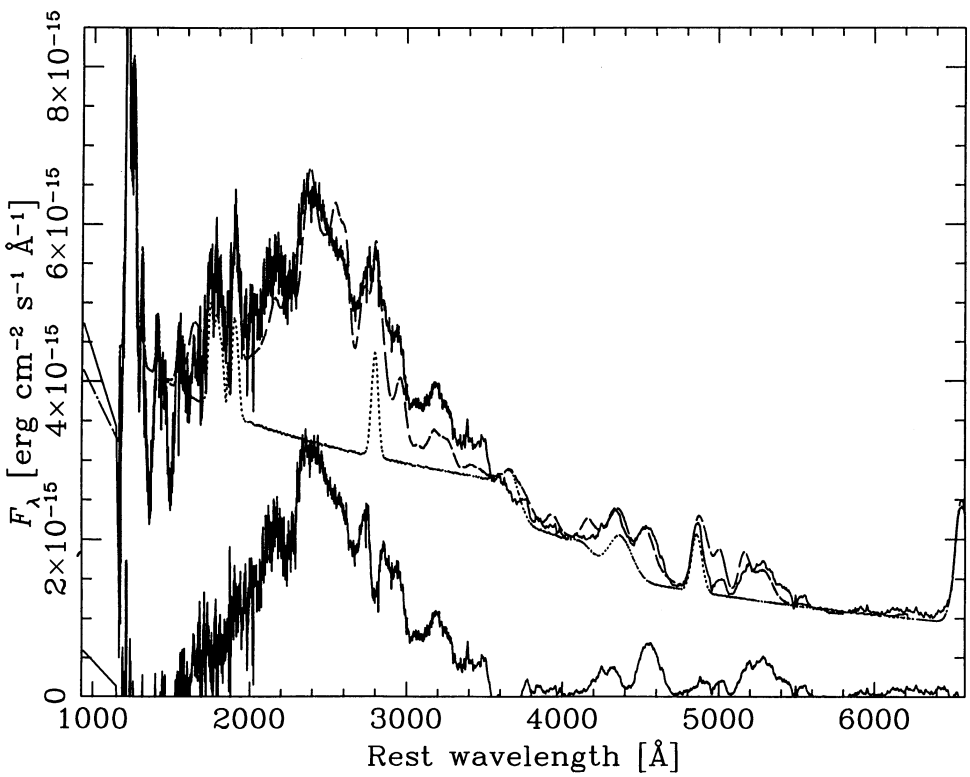

FIG. 7*b*

FIG. 7.—(*a*) Illustration of how the various components are fitted to the data for the case of an underlying power-law continuum. The final fit (*dashed curve*) to the data (*upper solid curve*) includes the resultant Fe II emission template plus power-law, Balmer and Paschen continua, and non–Fe II emission lines. The underlying power-law continuum was shown on Fig. 6*a*. The curve beneath the data (*dotted curve*) shows only the power-law, Balmer, and Paschen continua, and non–Fe II emission lines. A subtraction of the dotted curve from the data results in an empirical determination of the Fe II emission (*lower solid curve*) which can be measured (see Table 2). See the discussion in §§ 3.1 and 3.2. (*b*) Illustration of how the various components are fitted to the data for the case of an underlying power-law plus accretion disk continuum. The final fit (*dashed curve*) to the data (*upper solid curve*) includes the resultant Fe II emission template plus power law, accretion disk, Balmer, and Paschen continua, and non–Fe II emission lines. The underlying power-law plus accretion disk continuum was shown on Fig. 6*b*. The curve beneath the data (*dotted curve*) shows only the power-law, accretion disk, Balmer, and Paschen continua, and non–Fe II emission lines. A subtraction of the dotted curve from the data results in an empirical determination of the Fe II emission (*lower solid curve*) which can be measured (Table 2). See the discussion in §§ 3.1 and 3.2.

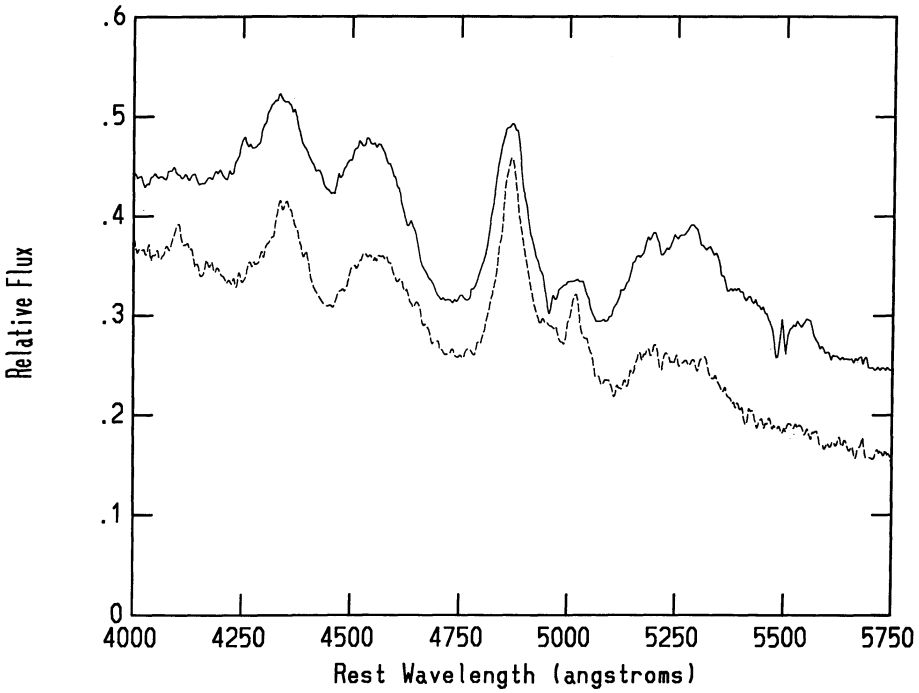

FIG. 8*a*

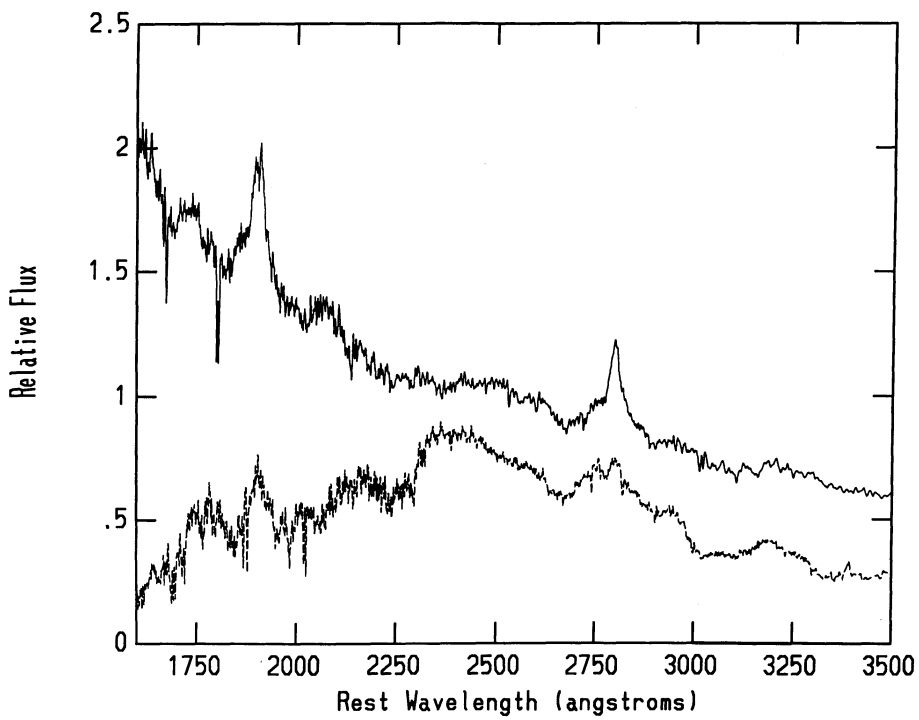

FIG. 8*b*

FIG. 8.—(*a*) Comparison of the spectrum of PG 0043+039 (*top*) to that of NGC 2841–UB 3 (*bottom*), another Key Project QSO, showing the strength of the Hβ and the optical Fe II emission. Both spectra have been shifted to rest frame wavelengths, and the spectrum of NGC 2841–UB 3 has been displaced downward slightly in flux. (*b*) A comparison of the PG 0043+039 spectrum (*bottom*) to that of NGC 2841–UB 3 (*top*) as in (*a*), but showing the region of the UV Fe II emission. The spectrum of PG 0043+039 has been displaced downward slightly in flux. Although the UV Fe II emission ($\sim$2250–2650 Å) of NGC 2841–UB 3 is very much weaker than in PG 0043+039, it is clearly present, and it is only moderately weaker than derived from the LBQS composite spectrum.

uum which may include substantial Fe II emission. The rest equivalent widths are also tabulated relative to the various underlying continuum models which do not include the Fe II emission or the Balmer and Paschen continua. In these cases the Fe II emission was removed by subtracting the theoretical Fe II emission spectrum template (§ 3.2.1). By using measurements of the Hβ emission-line flux reported in Table 2, some information on the observed and dereddened emission-line flux strengths for these transitions could be derived from the reported rest equivalent widths for the various continuum models. Finally, we give the equivalent width measurements for the LBQS composite spectrum for comparison. Some transitions are not tabulated because they are either too weak to identify or reliably measure given the strong Fe II emission in the spectrum.

Aside from the very strong Fe II emission, the noteworthy characteristics of the PG 0043+039 emission-line spectrum are (1) the absence of narrow-line emission from [O II] λ3727 and [O III] $\lambda\lambda$4959, 5007, (2) the absence of He II λ4686 emission, (3) the weakness of C IV $\lambda\lambda$1548, 1550 emission, (4) the strong emission feature near $\sim$1260 Å (possibly due to Si II), (5) a very strong emission feature near $\sim$1309 Å (also possibly due to Si II), (6) a FWHM of $\sim$3200 km s^{-1} for the Mg II BEL, and (6) a FWHM of $\sim$4500–8000 km s^{-1} for most of the other prominent BELs (e.g., Lyα, N V λ1260, Hβ), including Fe II.

The strength of the emission near the 1700–2000 Å region in PG 0043+039 is consistent with the interpretation put forth by Hartig & Baldwin (1986) in their study of BAL QSOs and, in particular, their analysis of the spectrum of the narrow emission-lined BAL QSO Q0335−336. Our analysis suggests that the emission near $\sim$1900 Å in PG 0043+039 may be due to Fe III UV34 or Si III λ1895 and C III] λ1909, while the emission near $\sim$1790 may be due to a combination of N III] λ1749, Fe II UV 191, and Si II λ1814. The presence of both Fe III UV 34 and Fe II UV 191 (e.g., as applied to the case of QSO Q0335−336) may be understood in the context of a model for the formation of Fe II UV 191 by Johansson & Hansen (1988). These authors have argued that the most likely mechanism for the production of Fe II UV 191 emission is by dielectronic recombination from Fe^{+2}. Since the most probable emission lines from Fe^{+2} are the Fe III UV 34 multiplet near 1900 Å, this lends support to the Fe III UV 34 identification. Production of UV 191 requires the simultaneous presence of high levels of excitation together with a high enough density to permit its formation. As neither the Fe II UV 191 nor Fe III UV 34 are generally seen in QSO/AGN spectra, the presence of such emission in some BAL QSOs raises the question of whether fundamental differences in the broad emission-line regions of these objects results in or is caused by the outflowing BAL region gas. The lines near $\sim$1780 Å, which are also present in the Q0336−336 spectrum, can be identified with a N III] doublet at $\sim$1749 Å and a Si II multiplet at $\sim$1814 Å. The presence of Si II in so strong an Fe II emitter is perhaps not surprising given the similarity of the Si^+ and Fe^+ ionization potentials, and this is why we suspect that the emission lines near $\sim$1260 Å and $\sim$1309 Å may be Si II. The presence of N III] in PG 0043+039 would suggest that the density is $\lesssim 10^{10}$ cm^{-3} in the region producing it, but if the Fe III UV 34 identification is correct, then this suggests that C III] may be very weak or absent. Since the critical density for the formation of C III] is slightly lower than that for N III], the observations may indicate that the emitting gas spans a narrow range of densities which is slightly higher than is representative for more normal QSOs which usually exhibit C III].

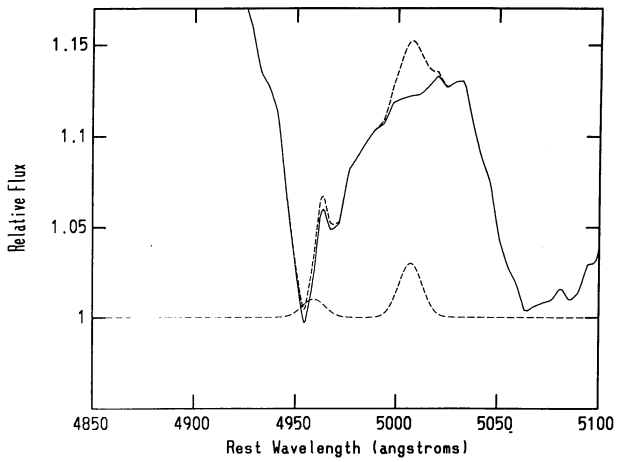

FIG. 9.—Enlargement of the rest frame spectrum shown in Fig. 1 around the predicted position of [O III] $\lambda\lambda$4959, 5007. The solid line is the observed flux from PG 0043+039. The upper dashed line is a simulated spectrum formed by adding [O III] $\lambda\lambda$4959, 5007 emission to the observed spectrum. The [O III] is taken to have the form of two Gaussians having the same width as observed in the composite spectrum described in § 3.1.1. The lower dashed line shows the profile of the [O III] which has been added, superposed on unit continuum. From this simulation we estimate an upper limit to the equivalent width of [O III] λ5007 in PG 0043+039 is $\sim$0.4 Å.

Finally, as we will consider results on the strength of [O III]$\lambda\lambda$4959, 5007 narrow emission in § 4, of special interest here is placing a limit on the maximum strength of any [O III]. Figure 9 presents an enlargement of the spectrum shown in Figure 1 near the predicted position of the [O III]. Obviously, any flux due to narrow-line [O III] emission is exceedingly weak. We have tried to estimate an upper limit to the amount of [O III] present by superposing on the observation of PG 0043+039 Gaussians (with a ratio of 1:3) at $\lambda\lambda$4959, 5007 whose width is the same as that measured for the [O III] in the composite spectrum described in § 3.1.1. The composite spectrum was assembled from individual spectra taken with the same instrumental setup as that used for the [O III] region of PG 0043+039. The simulated [O III] shown in Figure 9 has an equivalent width of 0.4 Å, which is $\sim$5% of the [O III] in the composite spectrum. The study of Boroson & Green (1992) includes observations of PG 0043+039 and similar conclusions on the strength of [O III] were reached in their study.

3.3. *Column Densities of BAL Region Material*

The removal of the Fe II emission and the determinations of the most probable underlying continuum levels as discussed in § 3.2 permits us to define normalized continua in the regions of the predicted BALs. From these estimations we can derive or place upper limits on BAL region column densities. We use the technique specified by Grillmair & Turnshek (1987) to do this. The results of this exercise, which assumes that the BAL region clouds completely cover the continuum source and that the BALs are resolved at our spectral resolution, are shown in Figure 10 for the regions near C IV and Si IV. The analysis shows that there is firm evidence for only C IV and Si IV BALs (see the fits shown in Fig. 10), while only upper limits can be placed on the BAL region column densities that correspond to the Al II, Al III, and Mg II lines (the fits are not shown). The derived column densities and upper limits on column densities are reported in Table 4. The deduced total C^{+3} column density is $\sim 3.1 \times 10^{15}$ cm^{-2} which is a factor of $\sim$4 smaller than what is typical in a representative sample of 20 BAL QSOs (Grillmair & Turnshek 1987). The analysis shows that the

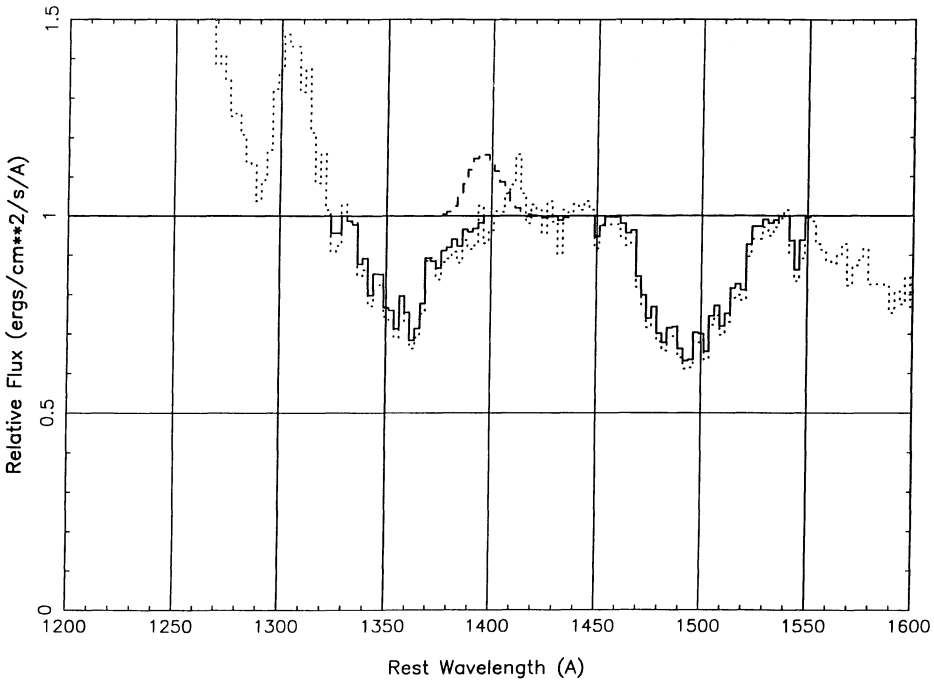

FIG. 10.—Based on a fitted continuum, the normalized BAL profiles are shown here in the region of C IV and Si IV as determined from the observations (*dotted lines*). The C^{+3} and Si^{+3} column densities are deduced from the fitted profiles (*solid lines*). Upper limits on the Al^{+}, Al^{+2}, and Mg^{+} column densities are derived in a similar manner (not shown). See the discussion in § 3.3.

Si^{+3}/C^{+3} column density ratio is ~ 0.25, while the Mg^{+}/C^{+3} column density ratio is $\lesssim 0.035$.

3.4. *Possible Brightness Variations*

Poor signal-to-noise ratio UV data of PG 0043+039 obtained in 1986 December and 1987 January have recently been included in the catalog of *IUE* spectra of QSOs and AGNs by Lanzetta et al. (1993). In addition, the earlier optical studies of Neugebauer et al. (1987), Baldwin et al. (1989), and Boroson & Green (1992) present optical spectrophotometry of PG 0043+039 over the wavelength intervals ~3200–9000 Å, ~3200–5300 Å, and 5950–7850 Å, respectively. The Neugebauer et al. data were obtained in the fall of 1980, the Baldwin et al. data were obtained in 1984 August (see Wampler & Ponz 1985), and the Boroson & Green data were obtained in 1990 September. All of these data are represented as having reasonably accurate absolute spectrophotometry. The new *HST*-FOS and ground-based data overlap in wavelength with these earlier data.

With the aid of these earlier data, the brightness of PG 0043+039 can be compared at five different epochs, namely 1980.8 (the optical data of Neugebauer et al. 1987), 1984.7 (the optical data of Baldwin et al. 1989), 1986.9 (the *IUE* data published by Lanzetta et al. 1993), 1990.8 (the optical data of Boroson & Green 1992), and 1991.8 (this study). The data at all five epochs are illustrated in Figure 11. Comparison of these spectrophotometric datasets at five different epochs over ~11 yr, which is ~8 yr in the QSO rest frame, tentatively indicates that PG 0043+039 has varied in brightness by as much as ~1.1 mag during this time interval. We consider evidence for this rather large variation (>1 mag) tentative because it is based solely on the Baldwin et al. results and the accuracy of optical spectrophotometry is often difficult to assess. Since the signal-to-noise ratio of the *IUE* data are especially low in the C IV region, we cannot make an assessment of possible variations in BAL strength with time. On the other hand, a comparison of the *IUE* and *HST* data indicates that a drop in brightness of ~0.5 mag did occur between 1986.9 and 1991.8.

TABLE 4

BAL REGION COLUMN DENSITIES[a]

Species	Column Density (cm^{-2})
C^{+3}	$3.1(10^{15})$
Si^{+3}	$7.7(10^{14})$
Al^{+}	$<3.8(10^{14})$
Al^{+2}	$<3.0(10^{14})$
Mg^{+}	$<1.1(10^{14})$

[a] Total column density of designated ion in the outflow velocity interval 5000–17,000 km s^{-1} measured by assuming that the BAL region clouds completely cover the fitted continuum model and that the absorption is kinematically resolved at the obtained spectral resolution.

4. DISCUSSION

4.1. *The BAL Region Covering Factor*

Most of the striking properties that PG 0043+039 exhibits—the lack of narrow-line [O III] emission in its spectrum, the very strong Fe II emission, and a strong deficit of flux in the UV shortward of ~2200 Å—are properties shared by the BAL QSOs which show low-ionization BALs (Weymann et al. 1991; Sprayberry & Foltz 1992; Boroson & Meyers 1992; Voit et al. 1993). What makes PG 0043+039 unique is that it has much weaker C IV BALs than are typical for the low-ionization BAL QSOs, and more important, it does not show any clear evidence for the low-ionization BAL troughs them-

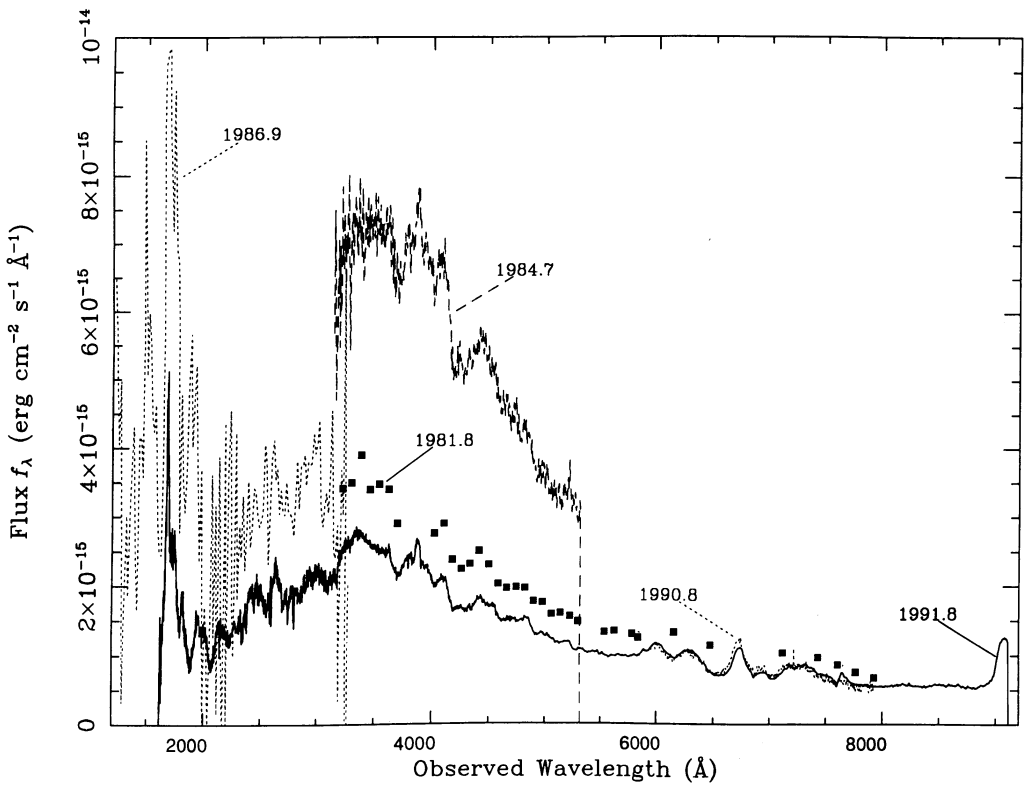

FIG. 11.—Evidence for possible variations in the PG 0043+039 flux as measured at five basically distinct epochs is shown by superposing the Neugebauer et al. (1987) data obtained in 1981.8, the Baldwin et al. (1989) data obtained in 1984.7, the Lanzetta et al. (1993) *IUE* data obtained in 1986.9 the Boroson & Green (1992) data obtained in 1990.8, and the *HST*/optical data obtained in 1991.8 for this study. See the discussion in § 3.4.

selves. We suggest therefore, that while there is evidence, as discussed below, that the low-ionization BAL region covering factor and the overall BAL region covering factor in a subset of QSOs is a substantial fraction of unity, it is not actually unity[14]. One can imagine that there will be a few objects which are intrinsically low-ionization BAL QSOs but for which the sight-line to them does not intersect BAL clouds having high enough column densities to produce observable low-ionization transitions (e.g., Al III and/or Mg II) or even for which the sight line may avoid all BAL clouds. The sight line to PG 0043+039 may be representative of such cases. In particular, recall that for PG 0043+039 we find $Mg^+/C^{+3} \lesssim 0.035$ (§ 3.3). However, in the low-ionization BAL QSO Q1232+134, which has C^{+3} column density ~ 7 times larger than observed in PG 0043+039, the Mg^+/C^{+3} ratio is ~ 0.035 (Kopko & Turnshek 1990; Kopko 1994), and so the column densities along our line of sight to PG 0043+039 may simply be too low to observe the low-ionization transitions.

As pointed out in the introduction, however, a fundamental problem with interpreting low-ionization BAL QSOs as high covering factor objects arises in trying to reconcile such a conclusion with the small fraction of QSOs which exhibit low-ionization BALs and with constraints from scattering arguments which indicate that BAL region covering factors are small (Hamann et al. 1993). Estimates which put the fraction of optically selected QSOs with BALs at $\sim 10\%$ and the fraction of optically selected QSOs with low-ionization BALs at $\sim 1\%$ may be used as a starting point for considering the value of the covering factor. For example, under the assumption that the narrow-line [O III] emission and the continuum are emitted isotropically and that the low-ionization BAL region covering factor is ~ 0.01, i.e., similar to the fraction of QSOs with low-ionization BALs, then there should be ~ 100 times as many QSOs similar to the low-ionization BAL QSOs, but which do not exhibit low-ionization BALs, as those which do. Since this is clearly not the case we could more conservatively consider the scattering constraints which typically require the covering factor to be $\lesssim 0.2$ under the assumption that the scattered photons are not destroyed. In this scenario there should be more than 4 times as many QSOs with properties similar to the low-ionization BAL QSOs but which do not exhibit low-ionization BALs. As discussed below, this possibility is not as easily ruled out. PG 0043+039, which does not clearly exhibit low-ionization BALs, may fit into this category. Finally, the most direct evidence for a large covering in the low-ionization BAL QSOs comes from the analysis of a sample of 19 QSOs selected from the *IRAS* Warm Extragalactic Object sample by Boroson & Meyers (1992). This sample includes four objects which could be classified as low-ionization BAL QSOs and all have [O III] emission equivalent widths $\lesssim 2$ Å. With the exception of 3C 273, which has an [O III] emission equivalent width of ~ 4 Å (5 Å as reported by Boroson & Green 1992), none of the other objects in the Boroson & Meyers sample had weak [O III].[15] This is suggestive of a low-ionization BAL region

[14] The term "low-ionization BAL region covering factor" should be distinguished from the more general term "BAL region covering factor." The first case refers to the fraction of the sight lines which would exhibit low-ionization BALs, while the latter term refers to the fraction of the sight lines which would exhibit any BALs.

[15] For our purposes here, we will define weak [O III] QSOs as objects with [O III] rest equivalent widths < 5 Å.

covering factor near unity in the weak–[O III], *IRAS*-selected objects. Recall, however, that PG 0043+039 itself was not detected with *IRAS* (§ 2.3) and the contradiction between a covering factor near unity and lack of scattered photons would be somewhat ameliorated because the BALs are very weak (§ 3.3), so that even with a large covering factor there would not be a large amount of resonance line scattered flux or collisionally excited flux from the BAL region as long as the BALs are weak along the other sight lines.

However, consideration of the properties of the *non-IRAS selected* PG sample of Boroson & Green (1992) yields somewhat different results on the value of the covering factor. The Boroson & Green sample of 87 QSOs includes 10 weak–[O III] QSOs. From this weak–[O III] sample we can form a subsample of six objects (including PG 0043+039) which have $z_{em} > 0.2$. This redshift limit permits an optical search for Mg II BALs. From the observations of Baldwin et al. (1989), we conclude that only one of the six objects (PG 1700+518) is a low-ionization BAL QSO. This would lead to an uncertain estimate of ~ 0.17 for the value of the low-ionization BAL region covering factor in this subsample, which is consistent with the scattering arguments providing the overall BAL region covering factor is not much larger. However, we can form another subsample of five weak–[O III] objects which have UV observations of sufficient quality (see Lanzetta et al. 1993) to permit a search for C IV BALs. Three of these five objects exhibit C IV BALs, leading to an estimate of ~ 0.6 for the value of the overall BAL region covering factor in this particular subsample. Whether the various results on covering factors between the different samples and subsamples is due to small-number statistics or a real physical difference in properties is not yet clear. On the one hand, the statistics may simply indicate that QSOs with weak–[O III] emission have low-ionization BAL region covering factor of ~ 0.2 and overall BAL region covering factor of ~ 0.6. However, if the low-ionization BAL region covering factor and far-IR flux emission are indeed correlated, this suggests that the weak–[O III], *IRAS*-selected QSOs can preferentially have very large low-ionization BAL region covering factors (i.e., $\gg 0.2$).

Thus, while the evidence concerning the actual value of the covering factor is mixed, *in the absence of a mechanism which would prevent* [O III] *emission from escaping the QSO in the direction of BAL region clouds or which would cause enhanced continuum and broad-line emission in the direction of BAL region clouds, there is clear evidence for larger overall and low-ionization BAL region covering factors in subsamples of weak–*[O III] *QSOs than is indicated by the scattering constraints.* Moreover, there are examples of low-ionization (Mg II) BAL QSOs with huge C IV absorption troughs and virtually no detectable C IV emission (e.g., see the spectrum of the low-ionization BAL QSO Q0059−2735 in Voit et al. 1993). Given the evidence for a large covering factor, an object with BALs like the ones observed in Q0059−2735 would be unlikely to exhibit such a small emission-to-absorption ratio unless there were destruction of scattered photons. As emphasized by Voit et al., some mechanism for destroying the scattered photons seems to be required.

4.2. *Suppression of* [O III] *Emission*

Aside from the questions involving the covering factor and scattering of photons, there remains the related questions of what mechanism suppresses the [O III] in low-ionization BAL QSOs and in QSOs in general. Boroson & Meyers suggest that either a "dusty torus" or the Mg II BAL clouds themselves may be the attenuating material that prevents the ionizing photons from reaching the narrow-line region. Once again assuming that the narrow-line [O III] emission and the continuum are emitted isotropically, the covering factor for the attenuating material must be nearly unity in order to suppress the [O III] significantly. As an illustration of this, in § 3.2.3 we estimated that the [O III] strength in PG 0043+039 was less than $\sim 5\%$ of that in the composite spectrum, implying that a covering factor for the attenuating material of ~ 0.95 was needed.

A variant of the "dusty torus" suggestion may provide a mechanism for destroying resonance line scattered photons. Voit et al. (1993) suggest that dust having an absorption optical depth of order unity at the wavelength of some resonance line could be effective in suppressing the emission lines. Only a modest line-of-sight optical depth for the dust would be required to significantly increase the effective optical depth for resonance line photons, but how this mechanism could destroy line photons observed on the long wavelength sides of the line centers is unclear. The mechanism would require, of course, that the dust not be localized in the higher density, lower ionization regions, where it presumably formed, but that it be distributed throughout the region where most of the optical depth in high-ionization BALs resides. Using the same line of reasoning as will be put forth in the next paragraph, this mechanism would require the "dusty torus" to have a significant optical depth below the Lyman limit.

In the case of the second of these two possibilities—attenuation of ionizing photons by continuous opacity of hydrogen and helium in the Mg II BAL material—high optical depths in the He II Lyman limit would probably enhance [O III] rather than suppress it, since the He II Lyman limit occurs just at the ionization potential of O^{+2}, so that very little of the oxygen would be in ionization states higher than O^{+2}. Thus, we must rely on Lyman continuum absorption from the H I and He I. We estimate that the contributions of H I and He I to the continuous opacity at the ionization potential of O^{+} (35 eV) are comparable, so that a total optical depth in the continuum of order 1 to 2 at 35 eV necessarily requires a very large optical depth at the H I Lyman limit, thereby ensuring suppression of O II as well. But as the models of Voit et al. (1993) demonstrate, such large optical depths at the H I Lyman limit should produce very strong Mg II. However, the existence of at least five weak–[O III] objects in the Boroson & Green PG sample which do not show Mg II BALs poses a problem. Since the low-ionization BAL region covering factor must be large for this mechanism, we should expect few, if any, weak–[O III] objects not to show strong Mg II BALs, contrary to what is found in the Boroson & Green PG sample. Depending on the details of the specific "dusty torus" model (e.g., such as the actual covering factor of the "dusty torus"), it may or may not suffer from such a problem.

Other possible explanations for the weak–[O III] found in some QSOs—and, as far as is known, in all low-ionization BAL QSOs—remain to be explored. One possibility is simply the absence of low-density gas, possibly because of expulsion by winds. How this mechanism could lead to the strong anti-correlation between the [O III] and Fe II strengths is unclear.

Alternatively, some mechanism may prevent narrow-line [O III] emission from escaping the QSO in the direction of the BAL region clouds while allowing it to escape along other directions. Netzer & Laor (1993) have argued that dust may be

embedded in the narrow-line emitting gas and hence the line-emission from *individual* narrow-line region clouds is highly nonisotropic. How such a mechanism could be incorporated into a reasonable geometry which would prevent the integrated narrow-line emission from escaping in the direction of BAL region clouds is hard to envisage. Hes, Barthel, & Fosbury (1993) have made the suggestion that a significant component of the [O III] line may arise in the nuclear region and that it may be subject to obscuration, causing the integrated [O III] emission to be anisotropic. This is another effect which might play some role.

Finally, a mechanism for producing greatly enhanced continuum and broad-line emission as well as strong Fe II emission along sight lines which pass through BAL region clouds could explain the small [O III] equivalent widths. For example, one scenario for enhanced continuum emission occurs naturally when observing an accretion disk face-on (Laor & Netzer 1989; Francis 1993). We showed in § 3.1.2 that the power law plus face-on accretion disk model similar to the one of Laor (1990) could be fitted to the PG 0043+039 observations without requiring intrinsic dust reddening. Thus, a possible mechanism may involve opposite cones of BAL region clouds which are outflowing perpendicular to the accretion disk. However, such a model would have to give rise to a factor of 10–20 enhancement of the continuum and the broad emission lines (and possibly even a stronger enhancement of the Fe II emission) in order to be viable, and this is rather large. In the anisotropic emission models a simple derivation of the value of the BAL region covering factor from statistics on the presence of BALs in the weak–[O III] QSOs would not be valid. The general conclusion would be that the spectral properties of QSOs are aspect-angle dependent, as has often been suggested.

4.3. *Intrinsic Dust Reddening?*

The analysis of § 3.1 shows that the continuous energy distribution of PG 0043+039 may be explained by invoking an intrinsic dust reddening model, but alternative models such as the steep power-law model or power-law plus accretion disk model cannot be ruled out. One caveat with respect to the proposal that the turndown in the UV continuum in PG 0043+039 is due to intrinsic dust extinction is that the dust-to-gas ratio (or more specifically the dust-to-C^{+3} ratio) may be abnormally large. In particular, the shape of the PG 0043+039 spectrum was found to be consistent with SMC-like dust with $E(B-V)=0.11$, despite a lower than normal C^{+3} column density. For comparison, Sprayberry & Foltz (1992) obtained a similar $E(B-V)$ but in a sample which had C^{+3} column densities which were ~ 5 times larger. According to Pei (1992), SMC-like dust with $E(B-V)=0.11$ would be indicative of an H I column density in the SMC of 4.4×10^{21} cm^{-2} with abundances that were ~ 0.5 times solar values. However, we would not necessarily expect such a large gas column along the sight line to PG 0043+039 because radiation pressure may have caused dust which was present in higher density and column density regions to drift into our line-of-sight (e.g., see Laor & Draine 1993 for some constraints on such a process). If a high column of gas lies along the sight line to PG 0043+039, it may or may not produce an observable Lyman limit, depending upon the ionization parameter. At least one BAL QSO with weak low-ionization BALs (Q0932+501) was recently observed with *HST*, and it is not optically thick at Lyman limit (Turnshek et al. 1994).

If the covering factor of the putative dusty region in PG 0043+039 is large, one would expect the infrared luminosity to be comparable to the luminosity lost as a result of the reddening (see Fig. 4). Thus, in principle, the *IRAS* limits (see Fig. 3) could be used to constrain the covering factor of any dusty region. At the same time, it should be noted for comparison that the *IRAS* source Q0759+6508 (Low et al. 1988; Lipari, Terlevich, & Macchetto 1993) is a low-redshift, low-ionization BAL QSO (see the *IUE* spectrum of Lanzetta et al. 1993) which also has very strong Fe II emission; it has an IR to optical luminosity ratio of ~ 5 (Low et al. 1988). For PG 0043+039, however, the IR to optical luminosity ratio is probably <1.

4.4. Fe II *Energy Budget Problem*

In § 3.2 we discussed various measurements of the exceedingly strong Fe II emission which is present in the PG 0043+039 spectrum. As reviewed by Netzer (1988, 1990), the presence of strong Fe II emission creates an energy budget problem in QSOs/AGNs, with an emission flux ratio of Fe II (total)/H$\beta \simeq 10$ being exemplary of the problem. See also Wills (1988) and Lipari et al. (1993) to make a comparison between other objects and the measurements we present in Table 2. Netzer suggests that models with enhanced Fe abundance may fit the observations best. In PG 0043+039 the problem appears to be ~ 5–6 times more severe than what is recognized as normal. We simply wish to point out that an energy budget problem would exist in the high covering factor, intrinsic dust-extinction model that has been proposed. However, this problem could be lessened in a model with anisotropic Fe II and continuum emission where the Fe II emission is more strongly enhanced than the continuum.

5. CONCLUSIONS AND SUGGESTIONS FOR FUTURE WORK

Our study has led to a number of conclusions, each of which should be further studied with future observational or theoretical programs:

1. The mechanism responsible for the suppression of narrow-line [O III] emission in the low-ionization BAL QSOs and in QSOs in general needs to be understood. Possibilities include the absence of low-density gas, mechanisms which prevent narrow-line [O III] emission from escaping a QSO near the direction of outflowing BAL region clouds but which allow it to escape in other directions, processes or geometrical effects which produce greatly enhanced continuum, broad-line and Fe II emission in the preferred directions, and absorption of photons capable of producing O^{+2} by material which may be, but is not always, correlated with observable low-ionization BALs. The [O III]–Fe II anticorrelation, which was convincingly established by Boroson & Green (1992), also requires investigation.

2. An important issue which needs to be investigated with better statistical accuracy is the difference in the incidence of low-ionization BAL QSOs (and for that matter all BAL QSOs) in the weak–[O III], *IRAS*-selected QSO sample and in weak–[O III], optically selected samples. Objects which appear not to have Mg II BALs but have weak [O III] may have C IV BALs and flux deficits in the far UV, similar to PG 0043+039. Further investigation of the conjecture that the covering factor of low-ionization BAL material and the *IRAS* flux are correlated needs to be carried out. Resonance line scattering calculations, like the ones of Hamann et al. (1993) but which incorporate dust, should be carried out to model QSOs of this type to provide direct constraints on requirements for destroy-

ing resonance-line scattered photons and the value of the BAL region covering factor.

3. PG 0043+039 was found to have exceedingly strong Fe II emission, among the strongest cases known. The implications of such strong emission for the QSO energy budget has been stressed (e.g., Netzer 1988, 1990). The problem requires further investigation.

4. The dust-extinction proposal for the continuous energy distribution of low-ionization BAL QSOs should be quantitatively pursued, as should the related questions of whether dust can readily form in higher density regions of low-ionization BAL QSOs and, if it can, whether it can drift into and survive in the unshielded high-ionization regions. Such a model holds promise as the current data seem to be most consistent with the general picture of low-ionization BAL QSOs being young QSOs with high BAL region covering factors "in the act of casting off their cocoons of gas and dust," as suggested by Voit et al. (1993); see also a qualitatively similar discussion by Hazard et al. 1984. If dust extinction is the correct explanation, the apparent high dust-to-gas ratio in PG 0043+039 needs to be understood. Alternative explanations, such as enhanced continuum and broad-line region emission in the direction of BAL region cloud outflow which may be perpendicular to the accretion disk, need to be further considered in order to test the various ideas about anisotropic emission. As § 3.1.2 suggests, the alternatives cannot be ruled out.

5. Over an ~ 8 yr period in the QSO rest frame (11 yr in the observed frame) PG 0043+039 may have varied in brightness by as much as ~ 1.1 mag. Such slow variability might characteristically distinguish BAL QSOs from radio-quiet non-BAL QSOs. A program to monitor BAL QSO and non-BAL QSO brightness variations is underway at the Las Campanas Observatories, and this and similar programs need to be extended to cover rest frame time intervals up to ~ 5–10 yr in duration.

6. Spectral observations of PG 0043+039 at UV wavelengths would be helpful for a variety of reasons. First, UV observations would help us choose between the various models for the continuous energy distribution. Second, in the intrinsic dust-extinction model for which $E(B-V) \simeq 0.11$ was derived, UV observations will allow better constraints to be placed on the dust-to-gas ratio. Third, the results of our BAL region column density analysis indicate that $N(\mathrm{Si}^{+3}) \simeq 0.25N(\mathrm{C}^{+3})$. The deconvolved column density profiles track each other very well over the 5000–17,000 km s^{-1} velocity interval in which absorption is found. For the observed $\mathrm{Si}^{+3}/\mathrm{C}^{+3}$ ratio, photoionization models with solar abundances predict a significant Lyα BAL but a weak N V $\lambda\lambda$1238, 1240 BAL and UV spectra would allow this prediction to be checked, resulting in a test of the simple solar-abundance photoionization model as was done for Q0226−1024 (Korista et al. 1993). Fourth, the UV observations might also be used to place constraints on BAL profile variations which would be interesting in view of the possible brightness variations.

7. Finally, sensitive observations of PG 0043+039 in both the infrared and X-ray regions would be of importance given the correlation between low-ionization BAL QSOs and *IRAS*-selected objects and the possibility of photoelectric absorption of X-rays.

We thank J. Baldwin, T. Boroson and J. Sulentic for providing us with their published data in digital form, D. Sprayberry and C. Foltz for advice on their reddening work, and J. Bahcall, T. Boroson, G. Ferland, P. Francis, V. Khersonsky, G. Kriss, A. Laor, H. Netzer and M. Voit for helpful discussions. We also thank H. Netzer for providing us with the modified theoretical Fe II emission template which we used in some of the fits. We thank Sheflynn Sherer for preparation of the manuscript. Finally, we especially thank J. Bahcall for his comments on drafts of this manuscript and, as Principal Investigator, his superb organization of the Quasar Absorption Line Key Project. This work was partially supported by NASA contract NAG5-1618 and grant GO-2424.01 from the Space Telescope Science Institute, which is operated by the Association of Universities for Research in Astronomy, Inc., under NASA contract NAS5-26555. This research has made use of the NASA/IPAC Extragalactic Database (NED) which is operated by the Jet Propulsion Laboratory, California Institute of Technology, under contract with NASA.

REFERENCES

Arp, H. C. 1981, ApJ, 250, 31
Bahcall, J. N., et al. 1993, ApJS, 87, 1
Baldwin, J. A., Wampler, E. J., & Gaskell, C. M. 1989, ApJ, 338, 630
Barlow, T. A., Junkkarinen, V. T., & Burbidge, E. M. 1989, ApJ, 347, 674
Barlow, T. A., et al. 1992, ApJ, 397, 81
Begelman, M., de Kool, M., & Sikora, M. 1991, ApJ, 382, 416
Boroson, T. A., & Green, R. F. 1992, ApJS, 80, 109
Boroson, T. A., & Meyers, K. A. 1992, ApJ, 397, 447
Burstein, D., & Heiles, C. 1982, AJ, 87, 1165
Diplas, A., & Savage, B. D. 1993, preprint
Francis, P. J. 1993, ApJ, 405, 119
Grillmair, C., & Turnshek, D. A. 1987, in QSO Absorption Lines: Probing the Universe (Poster Papers), ed. J. C. Blades, C. Norman, & D. A. Turnshek (STScI), 1
Hamann, F., Korista, K. T., & Morris, S. L. 1993, ApJ, 415, 541
Hartig, G. F., & Baldwin, J. A. 1986, ApJ, 302, 64
Hazard, C., McMahon, R. G., Webb, J. K., & Morton, D. C. 1987, ApJ, 323, 263
Hazard, C., Morton, D. C., Terlevich, R., & McMahon, R. G. 1984, ApJ, 282, 33
Hes, R., Barthel, P. D., & Fosbury, R. A. E. 1993, Nature, 362, 326
Johansson, S., & Hansen, J. E. 1988, in Physics of Formation of Fe II Lines Outside LTE, ed. R. Viotte, A. Vittone, & M. Friedjung (Dordrecht: Reidel), 235
Junkkarinen, V. T., Burbidge, E. M., & Smith, H. E. 1987, ApJ, 317, 460
Kellermann, K. I., et al. 1989, AJ, 98, 1195
Kopko, M., Jr. 1994, Ph.D. thesis, in preparation
Kopko, M., Jr., & Turnshek, D. A. 1990, BAAS, 21, 1131
Korista, K. T., et al. 1992, ApJ, 401, 529
———. 1994, in preparation
Kwan, J. 1990, ApJ, 353, 123
Lanzetta, K. M., Turnshek, D. A., & Sandoval, J. 1993, ApJS, 84, 109
Laor, A. 1990, MNRAS, 246, 369
Laor, A., & Draine, B. T. 1993, ApJ, 402, 441
Laor, A., & Netzer, H. 1989, MNRAS, 238, 897
Lipari, S., Terlevich, R., & Macchetto, F. 1993, ApJ, 406, 451
Lockman, F., & Savage, B. D. 1994, in preparation
Low, F. J., Cutri, R. M., Kleinmann, S. G., & Huchra, J. P. 1989, ApJ, 340, L1
Morris, S. L. 1988, ApJ, 330, L83
Morris, S. L., et al. 1991, ApJ, 102, 1627
Netzer, H. 1988, in Physics of Formation of Fe II Lines Outside LTE, ed. R. Viotte, A. Vittone, & M. Friedjung (Dordrecht: Reidel), 247
———. 1990, in Proc. Saas-Fee Advanced Course 20, Active Galactic Nuclei, ed. T. J. L. Couvoisier & T. Mayor (Berlin: Springer), 57
———. 1993, private communication
Netzer, H., & Laor, A. 1993, ApJ, 404, L51
Netzer, H., & Wills, B. J. 1983, ApJ, 275, 445
Neugebauer, G., et al. 1987, ApJS, 63, 615
Oke, J. B., & Gunn, J. 1982, PASP, 94, 586
Pei, Y. C. 1992, ApJ, 395, 484
Savage, B. D., et al. 1993, ApJ, 413, 116
Schmidt, M., & Green, R. F. 1986, ApJ, 305, 68
Schneider, D. P., et al. 1993, ApJS, 87, 45
Sprayberry, D., & Foltz, C. B. 1992, ApJ, 390, 39
Stocke, J. T., Morris, S. L., Weymann, R. J., & Foltz, C. B. 1992, ApJ, 396, 487
Sulentic, J. W., Zheng, W., & Arp, H. C. 1990, PASP, 102, 1275

Sun, W., & Malkan, M. 1989, ApJ, 346, 68
Turnshek, D. A. 1988, in QSO Absorption Lines: Probing the Universe, ed. J. C. Blades, D. A. Turnshek, & C. Norman (Cambridge Univ. Press), 17
Turnshek, D. A., et al. 1987, in QSO Absorption Lines: Probing the Universe (Poster Papers), ed. J. C. Blades, C. Norman, & D. A. Turnshek (Baltimore STScI), 4
———. 1994, in preparation
Turnshek, D. A., Foltz, C. B., Grillmair, C. J., & Weymann, R. J. 1988, ApJ, 325, 651
Voit, G. M., Weymann, R. J., & Korista, K. T. 1993, ApJ, 413, 95
Wampler, E. J., & Ponz, D. 1985, ApJ, 298, 448
Weymann, R. J., Turnshek, D. A., & Christiansen, W. A. 1985, in Astrophysics of Active Galaxies and QSOs, ed. J. S. Miller (Mill Valley, CA: University Science Books), 333
Weymann, R. J., et al. 1991, ApJ, 373, 23
Wills, B. J. 1988, in Physics of Formation of Fe II Lines Outside LTE, ed. R. Viotte, A. Vittone, & M. Friedjung (Dordrecht: Reidel), 161
Wills, B. J., Netzer, H., & Wills, D. 1985, ApJ, 288, 94